OPEN ACCESS

April 2024
ISSN 1684-5315
DOI: 10.5897/AJB
www.academicjournals.org

ACADEMIC JOURNALS
expand your knowledge

About AJB

The African Journal of Biotechnology (AJB) is a peer reviewed journal which commenced publication in 2002. AJB publishes articles from all areas of biotechnology including medical and pharmaceutical biotechnology, molecular diagnostics, applied biochemistry, industrial microbiology, molecular biology, bioinformatics, genomics and proteomics, transcriptomics and genome editing, food and agricultural technologies, and metabolic engineering. Manuscripts on economic and ethical issues relating to biotechnology research are also considered.

Indexing

CAB Abstracts, CABI's Global Health Database, Chemical Abstracts (CAS Source Index) Dimensions Database, Google Scholar, Matrix of Information for The Analysis of Journals (MIAR), Microsoft Academic, Research Gate

Open Access Policy

Open Access is a publication model that enables the dissemination of research articles to the global community without restriction through the internet. All articles published under open access can be accessed by anyone with internet connection.

The African Journals of Biotechnology is an Open Access journal. Abstracts and full texts of all articles published in this journal are freely accessible to everyone immediately after publication without any form of restriction.

Article License

All articles published by African Journal of Biotechnology are licensed under the Creative Commons Attribution 4.0 International License. This permits anyone to copy, redistribute, remix, transmit and adapt the work provided the original work and source is appropriately cited. Citation should include the article DOI. The article license is displayed on the abstract page the following statement:

This article is published under the terms of the Creative Commons Attribution License 4.0
Please refer to https://creativecommons.org/licenses/by/4.0/legalcode for details about Creative Commons Attribution License 4.0

Memberships and Standards

Academic Journals strongly supports the Open Access initiative. Abstracts and full texts of all articles published by Academic Journals are freely accessible to everyone immediately after publication.

All articles published by Academic Journals are licensed under the Creative Commons Attribution 4.0 International License (CC BY 4.0). This permits anyone to copy, redistribute, remix, transmit and adapt the work provided the original work and source is appropriately cited.

Crossref is an association of scholarly publishers that developed Digital Object Identification (DOI) system for the unique identification published materials. Academic Journals is a member of Crossref and uses the DOI system. All articles published by Academic Journals are issued DOI.

Similarity Check powered by iThenticate is an initiative started by CrossRef to help its members actively engage in efforts to prevent scholarly and professional plagiarism. Academic Journals is a member of Similarity Check.

CrossRef Cited-by Linking (formerly Forward Linking) is a service that allows you to discover how your publications are being cited and to incorporate that information into your online publication platform. Academic Journals is a member of CrossRef Cited-by.

Academic Journals is a member of the International Digital Publishing Forum (IDPF). The IDPF is the global trade and standards organization dedicated to the development and promotion of electronic publishing and content consumption.

Contact

Editorial Office: ajb@academicjournals.org

Help Desk: helpdesk@academicjournals.org

Website: http://www.academicjournals.org/journal/AJB

Submit manuscript online http://ms.academicjournals.org

Academic Journals
73023 Victoria Island, Lagos, Nigeria
ICEA Building, 17th Floor,
Kenyatta Avenue, Nairobi, Kenya.

Editor-in-Chief

Editorial Board Members

Table of Content

Vol. 23(4), pp.131-141, April 2024
DOI: 10.5897/AJB2024.17662
Article Number: C2C919D72050
ISSN: 1684-5315

http://www.academicjournals.org/AJB

ACADEMIC JOURNALS
expand your knowledge

African Journal of Biotechnology

Full Length Research Paper

In vitro antifungal potential of citral and nanoencapsulated citral against *Fusarium oxysporum* f.sp. *lycopersici*

Portia Osei-Obeng[1]*, Leonard Muriithi Kiirika[2] and Aggrey Bernard Nyende[2]

[1]Department of Molecular Biology and Biotechnology, Pan African University, Institute for Basic Sciences, Technology and Innovation, Nairobi, P. O. Box 62000-00200, Kenya.
[2]Department of Horticulture and Food Security, Jomo Kenyatta University of Agriculture and Technology, Nairobi, P. O. Box 62000-00200, Kenya.

Received 6 March 2024; Accepted 4 April 2024

This study aimed to encapsulate citral in chitosan nanoparticles and test its antifungal activity, along with the nanoparticles, against *Fusarium oxysporum f.sp. lycopersici* (FOL), a soil-borne pathogen causing worldwide yield losses in tomato production. The nanoparticles were characterized using scanning electron microscopy (SEM), FT-IR, encapsulation efficiency (EE), loading capacity (LC), and in vitro release pattern. SEM images revealed a spherical morphology with particle sizes ranging from 33 to 301 nm. EE and LC ranged from 2.9 to 7.2% and from 0.6 to 1.3%, respectively. The in vitro release exhibited a controlled pattern. Citral completely inhibited FOL mycelial growth at 500 µg/mL, with MIC/MFC determined at 512 µg/mL, whereas the nanoparticles achieved maximum mycelial inhibition (27%) at 1000 µg/mL, with MIC at 4096 µg/mL. Our study reveals citral as a potent biofungicide against FOL; however, further research is required to assess its in vivo activity. Increasing concentrations of the nanoparticles and the addition of copolymers to the chitosan-tripolyphosphate system for encapsulation of citral may enhance its potential for use as an antifungal agent.

Key words: Chitosan, nanoencapsulation, citral, antifungal, *Fusarium oxysporum* f.sp. *lycopersici.*

INTRODUCTION

Fusarium oxysporum f.sp. lycopersici (FOL), a soil-borne fungus, is the phytopathogen responsible for causing fusarium wilt in tomatoes. This devastating disease leads to significant global losses in tomato yields in the field, greenhouses, and high tunnels (Devi et al., 2022). The pathogen can persist in the soil for extended periods, even without a host (Sharma et al., 2017). FOL primarily infects the roots of tomato plants and subsequently colonizes the vascular tissues, disrupting the function of xylem vessels and leading to wilting, stunted growth, and plant death (Kalleli et al., 2020).

Current management of the pathogen mainly relies on chemical fungicides such as carbendazim and prochloraz (Srinivas et al., 2019). However, due to the adverse environmental and health effects, there is a pressing need to explore and adopt alternative, sustainable, and

*Corresponding author. E-mail: obengoseiportia@gmail.com.

eco-friendly control methods that can be used either independently or integrated into management systems for *Fusarium* wilt in tomatoes (Sharma et al., 2017).

A wide array of organic compounds known as secondary metabolites are produced by plants, playing an essential role in their defense against biotic and abiotic stresses (Yang et al., 2018). Among these secondary metabolites, essential oils (EOs) have garnered significant attention and have been extensively researched for their antifungal activity against disease-causing fungi (Lammari et al., 2020). Essential oils (EOs) containing cinnamaldehyde, citral, eugenol, thymol, and carvacrol as active compounds have been identified as particularly effective in combating these microbes (Bassolé and Juliani, 2012). Citral, a major active compound found in lemongrass and *Litsea cubeba* essential oils, has been investigated for its antifungal potential against various phytopathogenic fungi, including some members of the *F. oxysporum* species (Kaur et al., 2019). Citral's antifungal activity has been attributed to its ability to penetrate the cell membrane, altering membrane permeability and leading to cell leakage and fungal death (Kaur et al., 2019).

However, citral's susceptibility to oxidation, poor solubility in water, high volatility, and poor stability when exposed to open conditions limit its use in its pure form, similar to most essential oils (Ma et al., 2020). Therefore, to fully harness the antifungal potential of citral in plant protection, its formulation in a suitable carrier for efficient delivery is imperative. Agricultural research has gradually shifted from conventional to novel technologies like nanotechnology to aid in plant protection and overall crop production. Nanotechnology is being investigated for various purposes, including plant hormone delivery, controlled release of agrochemicals, and bioremediation (Worrall et al., 2018). Nanoparticles can serve as plant protectants themselves or as carriers for agrochemicals and active compounds (Worrall et al., 2018). As carriers, they enhance shelf-life, improve water solubility, reduce toxicity, promote site-specific uptake to the target pathogen, and increase the efficacy, stability, and bioavailability of the active compounds (Worrall et al., 2018).

A wide range of nanomaterials exists for use as nanoparticle carriers, including organic (polymers, proteins, carbohydrates), inorganic (metals, metal oxides), or carbon-based materials (Oleandro et al., 2024). Zein, a hydrophobic plant protein-based nanomaterial, has been explored as a nanocarrier for plant protection (Liu et al., 2023). Zein nanoparticles have been utilized to encapsulate *Zataria multiflora* and tested against wheat-pathogenic fungi and bacteria (Rasteh et al., 2024). Nunes et al. (2024) also encapsulated orange essential oil in zein nanoparticles and investigated its efficacy against *Fusarium* incidence during agroecological maize seed storage, showing that the zein-encapsulated oil performed significantly better than the pure oil. Alginate, an organic nanomaterial, is a hydrophilic biopolymer derived from brown algae and some bacteria. Alginate alone as a polysaccharide has been explored in the control of *Alternaria solani and F. oxysporum f.sp. albedinis* in tomato and date palm, respectively (Dey et al., 2019; Bouissil et al., 2022). Santos et al. (2023) co-encapsulated tea tree oil and *Cucumis sativa* seed oil in an alginate matrix and evaluated the system's ability to inhibit microorganisms and prolong fruit shelf-life.

Chitosan, a biopolymeric nanomaterial derived from the deacetylation of chitin, has been extensively explored due to its non-toxicity, biodegradability, bioavailability, biocompatibility, safety, and inherent antimicrobial properties (Xing et al., 2015). The antimicrobial properties of chitosan have been demonstrated in plants such as tomatoes, kiwifruit, and apples (Abdel-Rahman et al., 2021; Beatrice et al., 2017; Kiirika et al., 2013). Mechanisms of action of chitosan's antimicrobial activity include the interaction of the positive amino groups with negatively charged microbial surfaces, leading to membrane damage and alteration of membrane permeability, as well as deposition onto the microbial surface, which prevents the entry of nutrients and the outflow of metabolites for excretion (Xing et al., 2015). Chitosan has been widely used in the encapsulation of essential oils (EOs) and active compounds such as clove essential oil, eugenol, thymol, nettle essential oil, *Nepta hormozganica, and Nepta dschuprensis* essential oils (Hadidi et al., 2020; Oluoch et al., 2021; Bagheri et al., 2021; Amighi et al., 2023). The small size, high surface area, and target-specific properties of nanoparticles make them more advantageous in plant protection as they allow penetration of pathogen membranes (Hoang et al., 2022).

Although citral has been encapsulated in solid-lipid nanoparticles, nano-lipid carriers, chitosan/carboxymethyl cellulose copolymer to form hydrogel microspheres, and nano-emulsion, to the best of our knowledge, there is little or no information on the encapsulation of citral in pure chitosan nanoparticles via ionic gelation and its utilization as an antifungal agent for plant protection. Furthermore, while the antifungal activity of citral has been tested against plant pathogens and even members of the *F. oxysporum* species complex, there is a lack of data regarding its specific effect on *F. oxysporum f.sp. lycopersici*. Therefore, this study aimed to synthesize and characterize citral-loaded chitosan nanoparticles and assess the antifungal activity of the nanoparticles and pure citral against *F. oxysporum f.sp. lycopersici.*

MATERIALS AND METHODS

Chemical reagents

Citral (purity: 95%), chitosan (low molecular weight, degree of deacetylation ≥90%), and resazurin sodium salt were purchased from Glentham Life Sciences (Corsham, UK). Sodium tripolyphosphate (TPP) was obtained from Sigma-Aldrich (Missouri, USA). Potato dextrose agar and broth were sourced from Scharlab

(Barcelona, Spain), and carbendazim was acquired from Solarbio Life Science (Beijing, China). Tween 20 and 80, ethanol (purity: 95%), glacial acetic acid, and hydrochloric acid (concentration: 35%) were obtained from Legacy Lab Africa (Nairobi, Kenya).

Fungal strain

The *F. oxysporum f.sp lycopersici* pathogen was obtained from the Kenya Plant Health Inspectorate Services (KEPHIS, Kenya). The pathogen was maintained on Potato Dextrose Agar (PDA) supplemented with 30 mg/mL streptomycin sulfate to inhibit bacterial growth. Slants of the pathogen were also prepared on half-strength PDA with glycerol for long-term storage purposes.

Synthesis of citral-loaded chitosan nanoparticles

Citral-loaded chitosan nanoparticles were synthesized using the ionic gelation method, following the procedure described by Hosseini et al. (2013) with slight modifications. To prepare a chitosan solution (1.5% w/v), chitosan was dissolved by shaking in aqueous acetic acid (1% v/v) at 25°C overnight for 24 h. In a 40 mL volume of chitosan solution, Tween 80 was added as a surfactant and stirred at 45°C for 2 h to obtain a homogeneous mixture. Citral at varying weights (0, 0.15, 0.30, 0.45, and 0.60 g) was gradually added to the above mixture and agitated for 20 min, resulting in chitosan-to-citral weight ratios of 1:0, 1:0.25, 1:0.50, 1:0.75, and 1:1.00, respectively. TPP (0.5% w/v) was then added drop-wise to the emulsion under continuous stirring, and agitation was carried out for 40 min. The formed nanoparticles were separated by centrifugation of the solution at 4000 rpm for 30 min at 25°C. The collected wet particles were washed three times with distilled water under the same centrifugation conditions. To ensure the formation of a homogeneous suspension, the cleaned wet particles were dispersed in 25 mL of distilled water using a probe sonicator in an ice bath for 4 min with a 2 s sonication and 1 s rest sequence. The resulting homogeneous suspensions were then freeze-dried at -65°C for 72 h. The freeze-dried nanoparticles were subsequently stored at 4°C until further use and analysis.

Characterization of nanoparticles

Determination of particle size and morphology

The size and morphology of the prepared nanoparticles were analyzed using a scanning electron microscope (FEI Helios NanoLab 600, Hillsboro, OR, NIST-USA), following the method described by Hosseini et al. (2013). Fourier-transform infrared spectroscopy (FTIR) analysis was conducted using an IRAffinity-1S FTIR spectrophotometer (Shimadzu Corp., 031891) equipped with an ATR to determine the functional groups on the surface of chitosan nanoparticles, citral, and the citral-loaded chitosan nanoparticles. The sample holder was filled with 1 mg of the sample, and the instrument was set up to perform a total of 20 scans with a 4 cm^{-1} spectral resolution for both background and sample spectra, recorded rapidly in the range between 4000 to 400 cm^{-1}.

Determination of encapsulation efficiency (EE %) and loading capacity (LC %)

The amount of citral encapsulated in chitosan nanoparticles was determined by UV-vis spectrophotometry following the method described by Hosseini et al. (2013). To achieve this, 10 mg of citral-loaded chitosan nanoparticles were mixed in 4 mL of 2M HCl and boiled at 95°C for 30 min. After cooling, 2 mL of ethanol was added to the homogeneous mixture and centrifuged at 9000 rpm for 5 min at 25°C. The supernatant was analyzed for citral content using UV-vis spectrophotometry at 298.5 nm. The amount of citral was calculated using the calibration curve of free citral (0.02, 0.04, 0.06, 0.08, and 0.10%) in absolute ethanol. Chitosan nanoparticles underwent a similar process as citral-loaded chitosan nanoparticles and were used as blanks. Each sample was recorded in triplicate. Loading capacity and encapsulation efficiency were estimated from Equations (1) and (2).

$$EE\% = \frac{\text{weight of loaded compound}}{\text{weight of initial compound}} \times 100 \quad (1)$$

$$LC\% = \frac{\text{weight of the loaded compound}}{\text{weight of NPs after freeze drying}} \times 100 \quad (2)$$

In vitro release study

The in vitro release study of citral from chitosan nanoparticles was conducted in different media (PBS and acetate buffer) at different pH (7.4 and 5), respectively, using the dialysis method as described by Shetta et al. (2019). Briefly, 40 mg of freeze-dried citral-loaded chitosan nanoparticles (1:0.50 w/w) was placed in a dialysis bag (12,000-14,000 kDa) containing 2 mL of the release media (PBS or acetate buffer) and placed in a 50 mL tube containing 13 mL of the same release media, incubated at room temperature under gentle shaking. At every time interval of 12 h, 5 mL of release media in the 50 mL tube was taken for analysis and an equal volume of fresh release media was added. The total cumulative amount of citral (mg) in the release medium (mL) volume encapsulated in the nanoparticles was quantified spectrophotometrically. The release was quantified as described by Oluoch et al. (2021):

$$\text{Release } \% = \frac{\text{Released oil}}{\text{Total oil}} \times 100 \quad (3)$$

Antifungal activity evaluation

Mycelial growth inhibition

The antifungal activity of pure citral and the citral-loaded chitosan nanoparticles (1:0.50 w/w chitosan to citral weight ratio) was assessed using the poisoned food technique described by La Torre et al. (2016). Citral and the nanoparticles were dissolved in 0.5% Tween 20 made with sterile distilled water. Potato dextrose agar (PDA) was prepared in distilled water and autoclaved at 121°C for 15 min, allowed to cool, and maintained at a molten state (45°C) in a water bath (45±1°C). The products (citral and nanoparticles) were then added to 20 mL of molten PDA and poured into 90 mm Petri dishes to achieve final concentrations of 250, 500, 750, and 1000 µg/mL. Carbendazim at 100 µg/mL dissolved in 0.5% Tween 20 was used as the positive control, and 0.5% Tween 20 was used as the negative control. After allowing the agar to solidify, the plates were inoculated at the center with 5 mm diameter mycelial plugs cut from the peripheral areas of a 7-day-old pre-cultured FOL. The plates were sealed with parafilm and incubated at 25±1°C until the growth in the control reached the edges of the plates. Percentage mycelial inhibition was calculated relative to the control using the

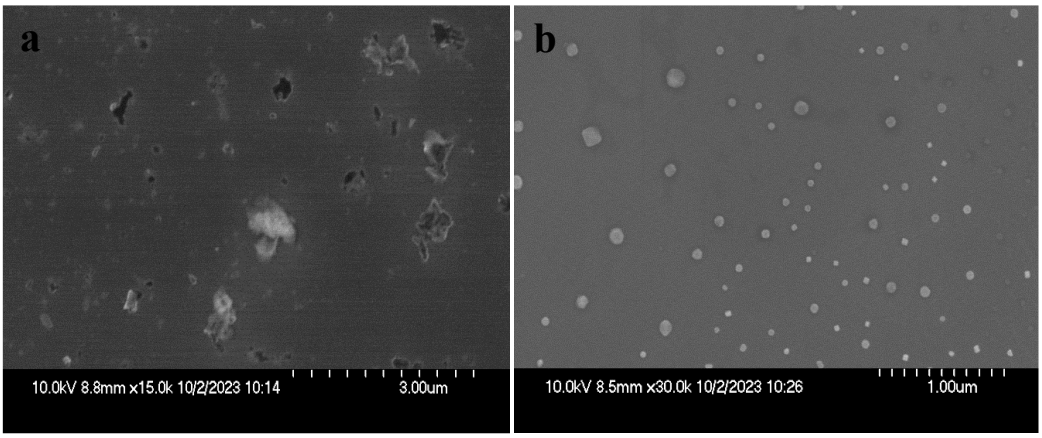

Figure 1. SEM micrograph of (a) chitosan nanoparticles and (b) citral-loaded chitosan nanoparticles made with chitosan to citral ratio of 1:0.50 (w/w).

formula proposed by Chun and Chandrasekaran (2019):

$$Percent\ Inhibition = \frac{(Mc - Mt)}{Mc} \times 100 \quad (4)$$

Where Mc is the mycelial growth in control and Mt is the mycelial growth in treatment.

Determination of minimum inhibitory and fungicidal concentrations

The broth micro-dilution method was employed to determine the minimum inhibitory concentrations (MICs) of citral and nanoparticles, as described by Sharma et al. (2017). The inoculum suspension was prepared by culturing *F.oxysporum f.sp. lycopersici* (FOL) at 25±1°C on Potato Dextrose Agar (PDA) for 7 days. The dishes were flooded with 10-15 mL sterile distilled water, and spores were carefully scraped off. The suspension was filtered through sterile cheesecloth to remove mycelial fragments, vortexed for 15 s to ensure homogeneity, and quantified using a hemocytometer. A final inoculum concentration of 2-2.5 × 10^5 cells/mL was used for the assay. Resazurin was prepared by dissolving 270 mg of the powder in 40 mL of sterile distilled water. A two-fold serial dilution ranging from 4096 to 8 µg/mL was prepared for both citral and nanoparticles. Each 100 µL of the dilutions received 20 µL of the inoculum suspension and 30 µL of resazurin. Positive control wells contained broth, inoculum suspension, and resazurin, whereas negative control wells contained only broth and resazurin to check the sterility of the broth. The plates were then incubated at 28±1°C for 48 h. The experiments were performed in triplicate, and the minimum inhibitory concentration was determined as the lowest concentration at which there was no color change. To determine the minimum fungicidal concentration (MFC), 10 µL of the wells with no color change were plated on PDA plates supplemented with 30 mg/mL streptomycin sulfate. The plates were incubated at 28±1°C for 72 h, and the lowest concentration at which no visible fungal growth was observed was taken as the MFC.

Statistical analysis

The average particle size was determined from SEM images using ImageJ 1.54d (http://imagej.org) and analyzed using Microsoft Excel 2013. Data on the effects of the treatments on the mycelial growth of *F. oxysporum f.sp. lycopersici* were analyzed using a one-way analysis of variance and means comparison using Tukey's test at a significance level of $p < 0.05$. The statistical analyses used R v.4.3.1 and Origin 2023 learning edition.

RESULTS AND DISCUSSION

Particle size and morphology distribution

The SEM images of the chitosan nanoparticles and the citral-loaded chitosan nanoparticles revealed irregular particle shapes and distributions, as depicted in Figures 1a and b. This irregularity in shape and distribution can be attributed to the potential instability encountered during the preparation process, as previously reported by Hosseini et al. (2013), and is consistent with the findings of Haider et al. (2017). Interestingly, the citral-loaded chitosan nanoparticles exhibited a distinctive spherical shape, while the unloaded chitosan nanoparticles appeared somewhat collapsed. This discrepancy in shape may be attributed to the reduced turgidity of the unloaded nanoparticles, resulting in instability of surface morphology, as suggested by Kalagatur et al. (2018). It's noteworthy that our observations deviated from some previous studies where chitosan nanoparticles encapsulating essential oil active compounds such as eugenol, thymol, and carvacrol displayed regular nanoparticle distributions and spherical shape for the unloaded chitosan nanoparticles, as reported by Keawchaoon and Yoksan (2011) and Oluoch et al. (2021).

The average size of the unloaded chitosan nanoparticles, as outlined in Table 1, was 99 nm. In contrast, the size of the citral-loaded chitosan nanoparticles exhibited a range from 33 to 301 nm, which notably falls within the acceptable size range (10 to 1000

Table 1. Average particle size of chitosan nanoparticles and citral-loaded chitosan nanoparticles and encapsulation efficiency (EE%) and loading capacity (LC%) of citral in citral-loaded chitosan nanoparticles by UV-Vis spectrophotometry.

Chitosan:citral ratio (w/w)	Average particle size (nm)[a]	EE (%)[b]	LC (%)[c]
1:0	99.00±34.00	0.00	0.00
1:0.25	94.00±29.00	5.20	0.60
1:0.50	301.00±130.00	7.20	0.90
1:0.75	72.80±26.83	4.00	1.03
1:1.00	33.32±5.93	2.90	1.31

[a] Results were reported as mean ± SD. [b,c] Results are means of triplicate data, and the standard deviation is 0.00.

nm) for nanoparticles fabricated with biopolymers like chitosan, as corroborated by Khanmohammadi et al. (2015). Unlike in previous studies where particle size increased as a function of increased oil content (Hosseini et al., 2013; Shetta et al., 2019), in this study, after the citral content of 0.50%, particle size began to decrease. This phenomenon may have been due to the interactions of the citral and the chitosan leading to more compact and smaller nanoparticles with an increase in initial citral content (Begines et al., 2020; Jia et al., 2020). However, particle size decreased with increased extract content in studies where plant extracts from Arrabidaea chia and Mentha longifolia were encapsulated in chitosan nanoparticles (El-Aziz et al., 2018; Servat-Medina et al., 2015). Additionally, a study on the encapsulation of krill oil in chitosan nanoparticles observed a similar phenomenon (Haider et al., 2017).

Fourier Transform Infrared Spectroscopy (FTIR) characterization

FTIR spectra of chitosan nanoparticles, citral, and citral-loaded chitosan nanoparticles (1:0.50 chitosan to citral ratio) are shown in Figure 2. Chitosan nanoparticles exhibited a characteristic broad peak at 3418 cm^{-1}, attributed to the presence of O-H and N-H stretching groups, a peak at 1535 cm^{-1} (amide II), and a peak at 1220 cm^{-1} (C-O-C stretch). These peaks indicate how the NH_3+ groups of chitosan and the phosphoric groups of the tripolyphosphate used as the cross-linker interact electrostatically to form the chitosan nanoparticles spontaneously (Hosseini et al., 2013).

Pure citral (95%) exhibited characteristic peaks at 2922 cm and 2856 cm^{-1}, which can be assigned to C-H stretching vibration, a strong absorption band at 1674 cm^{-1} (C=O stretching vibration), 1445 cm^{-1} (C=C vibration), and 1380 cm^{-1} (CH3 bending) (Zhu et al., 2015). The citral-loaded chitosan nanoparticles showed peaks that could be found in both the chitosan nanoparticles and pure citral (Figure 2c). The 2929 cm^{-1} (C-H stretching) peak present in the citral-loaded chitosan nanoparticles but absent in the chitosan nanoparticles indicates the increased ester groups, which may be from the citral, suggesting the successful encapsulation of citral into the chitosan nanoparticles (Keawchaoon and Yoksan, 2011). The shift of the peak at 1674 cm^{-1} in pure citral to 1734 cm^{-1} in the citral-loaded chitosan nanoparticles also indicates the presence of an ester group, which may have originated from the citral, further indicating the successful encapsulation of citral into the chitosan nanoparticles (Tian et al., 2018).

Encapsulation efficiency and loading capacity

Encapsulation efficiency (EE%) and loading capacity (LC%) of citral in the citral-loaded chitosan nanoparticles were determined using UV-Vis spectrophotometry. The maximum absorbance of citral was found at 298.5 nm, and a calibration curve (R^2 = 0.9749) was constructed for citral (0.02, 0.04, 0.06, 0.08, and 0.10%) in absolute ethanol. The percentages of EE and LC were calculated using Equations (1) and (2), respectively, as shown in Table 1. The EE% of citral ranged from 2.9 to 7.2%, with the maximum EE% achieved at 1:0.50 (w/w) chitosan to citral ratio. EE% decreased with increasing initial citral content, which may be attributed to the saturation point reached when loading citral into the chitosan nanoparticles, consistent with earlier findings (Haider et al., 2017; Hosseini et al., 2013; Shetta et al., 2019).

The relatively low encapsulation of citral might result from the hydrophobic nature of citral, posing challenges in achieving uniform dispersion within the chitosan solution and citral's instability in acidic environments (Maswal and Dar, 2014). Nevertheless, further optimization of the chitosan-tripolyphosphate encapsulation system parameters, the addition of copolymers, and the use of different nanocarrier system forms may enhance the encapsulation efficiency of citral (Jia et al., 2020; Khanmohammadi et al., 2015; Worrall et al., 2018). Conversely, LC% of citral ranged from 0.6-1.3%. Unlike EE%, LC% increased with the rise in initial citral content, consistent with observations made in

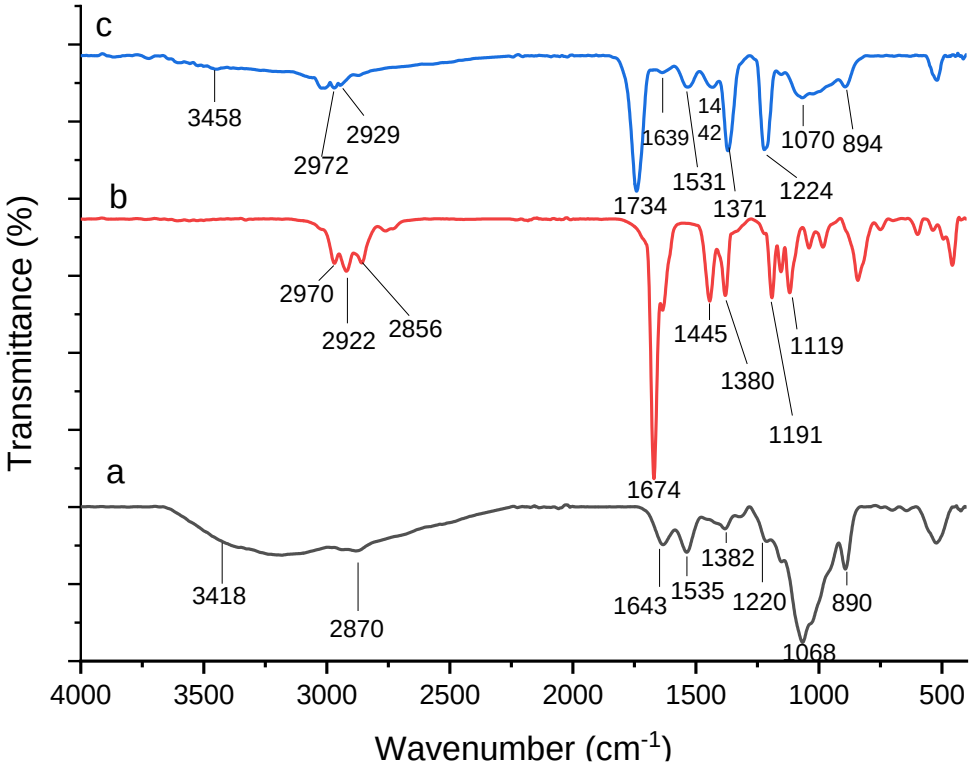

Figure 2. FTIR spectra of (a) chitosan nanoparticles, (b) citral and (c) citral-loaded chitosan nanoparticles with chitosan to citral weight ratio of 1:0.50 (w/w).

previous studies related to loading carvacrol and oregano essential oil into chitosan-TPP systems (Hosseini et al., 2013; Keawchaoon and Yoksan, 2011). The 1:0.50 (w/w) chitosan to citral ratio was chosen as the optimal formulation for the rest of the study.

In vitro release of citral from chitosan nanoparticles

The *in vitro* release investigation of citral from the citral-loaded chitosan nanoparticles (1:0.50 (w/w) chitosan to citral ratio) (Figure 3) was conducted in different pH media: PBS (pH 7.4) and acetate buffer (pH 5) for 72 h to confirm the successful encapsulation of citral in the chitosan nanoparticles and determine the ideal pH condition for the release of citral from the nanoparticles (Keawchaoon and Yoksan, 2011). Generally, diffusion, surface erosion, disintegration, and desorption are the various mechanisms by which a drug or oil is released from micro and nanoparticles (Hosseini et al., 2013). The release pattern of citral from chitosan nanoparticles can be described as a biphasic process with two distinct phases: an initial burst release followed by a subsequent sustained slower release, which aligns with previous findings related to the release of oregano, thymol, and eugenol from chitosan nanoparticles (Hosseini et al., 2013; Oluoch et al., 2021).

In the first 12 h, an initial burst release occurred, with citral being released up to 39.2 and 43.5% in PBS (pH 7.4) and acetate buffer (pH 5), respectively. This initial burst release may be attributed to the citral molecules attached to the surface of the nanoparticles and those encapsulated in proximity to the surface. As the dissolution rate of the polymer is elevated near the surface, there is also a substantial release of the drug, citral, in this study (Anitha et al., 2011). The release of citral in the second phase showed a slow release pattern, with citral being released up to 62.1 and 75.2% in PBS (pH 7.4) and acetate buffer (pH 5), respectively, at the end of the 72-h period. This slow release in the second phase could be attributed to the diffusion of citral from the chitosan nanoparticles (Oluoch et al., 2021). The release occurred more rapidly under acidic conditions compared to neutral conditions. In an acidic environment, the protonation of the amino groups on the surface of the chitosan nanoparticles causes the polymer matrix to swell, facilitating the quicker release of the drug (Anitha et al., 2011). These findings align with previous studies, where the release of carvacrol from the chitosan-TPP nanoparticles system and curcumin from dextran sulfate-chitosan nanoparticles in pH 3 and pH 5 showed a more rapid release than in neutral conditions (Anitha et al., 2011; Keawchaoon and Yoksan, 2011).

It is worth noting that the release of citral was not

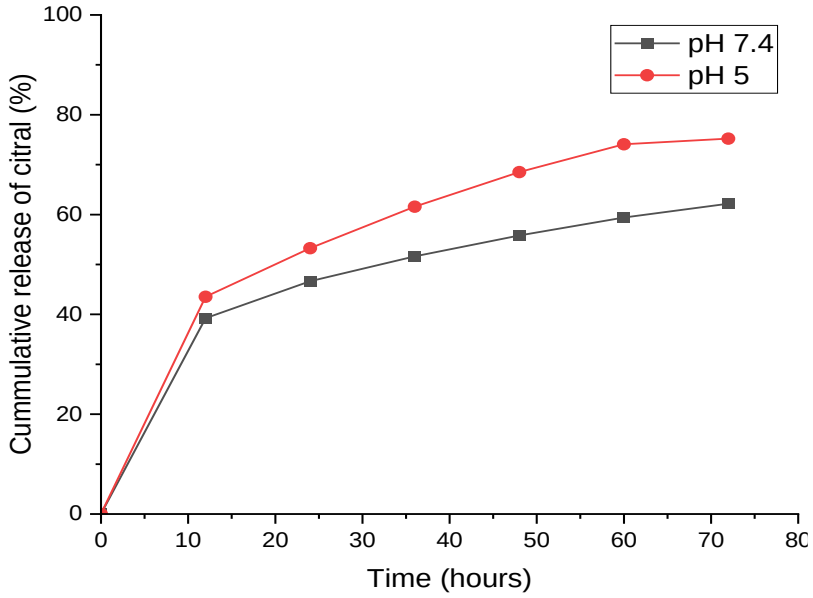

Figure 3. *In vitro* release profile of citral from chitosan nanoparticles in different pH media.

complete, as a complete release would require the total degradation of the chitosan nanoparticles (Shetta et al., 2019). Optimum tomato performance is achieved in a well-drained, light loam soil with a pH of 5 to 7, indicating that more than 70% of citral oil will be released in an ideal pH of 5 if used in field studies.

Mycelia growth inhibition

The results of the mycelial growth and inhibition assay of *F. oxysporum f.sp lycopersici* (FOL) by citral and citral-loaded chitosan nanoparticles are presented in Figure 4, and their values are reported in Table 2. Both citral and its nanoparticles exhibited inhibitory effects on FOL mycelial growth, albeit in a dose-dependent manner. The negative control (0.5% Tween 20) showed a mean growth of 85.7±0.67 mm (Figure 4C(j)), whereas the positive control (100 µg/mL carbendazim) completely inhibited the mycelial growth of the test fungus (Figure 4C (i)). Carbendazim, a broad-spectrum systemic fungicide, has been used to control fusarium wilt of tomatoes and other plant-pathogenic fungi (Ayesha et al., 2021). Yassin et al. (2021) revealed that carbendazim, at a low concentration of 0.50 ppm, could completely inhibit the mycelial growth of *F. proliferatum*. These previous findings demonstrate the effectiveness of carbendazim in managing fungal diseases; nevertheless, the World Health Organization classifies carbendazim as a hazardous chemical, hence the need to find more environmentally friendly ways of crop protection (Li et al., 2020).

Citral at a concentration of 250 µg/mL (Figure 4A(a)) showed mycelial inhibition of 40.5%. With increased concentrations (500, 750, and 1000 µg/mL) (Figure 4A(b, c, d)), it completely inhibited the growth of FOL, showing 100% mycelial inhibition (Table 2). This dose-dependent inhibition aligns with previous findings where citral was tested against plant fungal pathogens (Wei et al., 2021). Citral at a concentration of 20 µL/L inhibited the growth of *F. oxysporum* (Linde et al., 2010) completely. The study also demonstrated citral as being more active than the two essential oils used, suggesting citral as the main compound influencing the antifungal activity of the essential oils. Previous studies have shown that citral's antifungal potential may be due to its ability to cross the plasma membrane of phytopathogenic fungi and interact with the membrane's proteins and enzymes. Monoterpene-membrane protein interactions alter hyphae and plasma membrane morphology, causing fungal cell death (Kaur et al., 2019).

The maximum inhibition by the nanoparticles was recorded at 27.16% at a concentration of 1000 µg/mL. A comparison of the mycelial inhibition of pure citral and its nanoparticles showed a significant difference in mycelial inhibition, where citral proved more active and potent than its nano-encapsulated counterpart. This finding contrasts with previous research where nano-emulsions of citral exhibited higher antibacterial activity than pure citral (Marei et al., 2018). Sharma et al. (2023) encapsulated citral in chitosan nanoparticles prepared using chitosan sulfate, a derivative of chitosan, and their results showed that nano-encapsulated citral performed better than pure citral in quorum sensing inhibition. Kalagatur et al. (2018) reported improved antifungal activity of nano-encapsulated *Cymbopogon martinii*

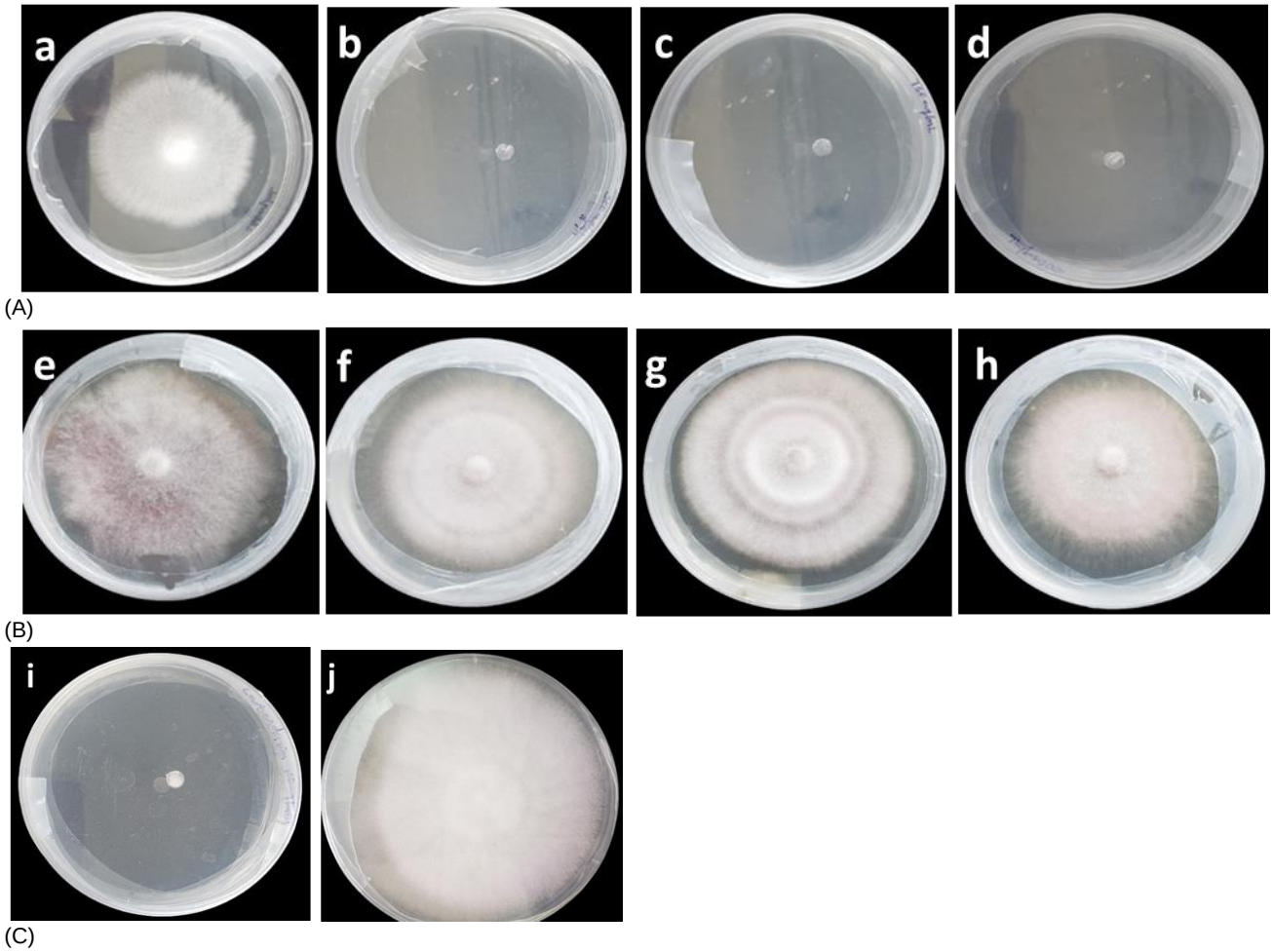

Figure 4. Mycelial growth inhibition of FOL plates treated with (A) citral: (a) 250µg/mL, (b) 500µg/mL, (c) 750µg/mL, and (d) 1000µg/mL; (B) citral-loaded chitosan nanoparticles (1:0.50 chitosan to citral weight ratio): (e) 250µg/mL, (f) 500µg/mL, (g) 750µg/mL and, (h) 1000µg/mL; (C) control: (i) 100µg/mL carbendazim and, (j) 0.5% Tween 20.

essential oil against *F. graminearum*. Cai et al. (2023) loaded *Athyrium sinense* essential oil against *Pectobacterium carotovorum sp. Carotovorum*, and the nanoparticles exhibited significant antibacterial activity against the pathogen. Thymol encapsulated in chitosan nanoparticles and tested against *Botrytis cinerea* by Zhao et al. (2023) also showed higher antifungal activity than unencapsulated thymol.

The significantly lower mycelial inhibition by the citral-loaded chitosan nanoparticles may be attributed to its low encapsulation efficiency (7.2%), as seen in Table 1, and perhaps a situation of incompatibility between the chitosan nanocarrier and citral oil, particularly during the ionic gelation process to form the nanoparticles. This antifungal activity may be improved if the concentration of the citral-loaded chitosan nanoparticles is increased, as demonstrated in Table 2, where an increase in nanoparticle concentration from 250 to 1000 µg/mL significantly increased mycelial growth inhibition. However, cost considerations may arise with increasing concentrations to boost antifungal activity.

Nonetheless, employing different encapsulation methods like coacervation, spray-drying, nanoprecipitation, or a combination of these methods could enhance the encapsulation efficiency of citral oil and subsequently increase its antifungal activity, as shown in previous studies (Lü et al., 2018; Jian et al., 2019). Furthermore, optimization of encapsulation parameters like pH, temperature, stirring speed, and time, the addition of copolymers like alginate, and the use of co-surfactants in the chitosan-tripolyphosphate encapsulation system could also help in improving the encapsulation efficiency of citral oil in the chitosan nanoparticles and ultimately its antifungal activity (Nagpal et al., 2010). Additionally, different carrier materials like zein and maltodextrin could be utilized for the encapsulation of citral oil to ensure the uniform dispersion of citral and enhance its encapsulation (Yammine et al.,

Table 2. Mycelia growth inhibition of different concentrations of citral and its nanoparticles against *Fusarium oxysporum* f.sp. *lycopersici*.

Treatment	Concentration (µg/mL)	Mycelial Growth (mm)	MGI%
Citral	250	51.00±0.58^{d}	40.50
	500	00.00±0.00^{e}	100.00
	750	00.00±0.00^{e}	100.00
	1000	00.00±0.00^{e}	100.00
CCNPs	250	75.70±1.20^{b}	11.68
	500	68.70±2.03^{bc}	19.80
	750	65.70±1.76^{c}	23.33
	1000	62.30±3.71^{c}	27.16
Carbendazim	100	00.00±0.00^{e}	100.00
Negative control	0.5% Tween 20	85.70±0.67^{a}	-

Values within columns followed by same letter are not significantly different by Tukey's test ($p < 0.05$). Results are means of 3replicates ±Standard Error (SE), MGI %: percent mycelial growth inhibition, CCNPs: citral-loaded chitosan nanoparticles (1:0.50 chitosan to citral weight ratio).

Table 3. Minimum inhibitory concentration (MIC) and minimum fungicidal concentration (MFC) of citral and its nanoparticles against *Fusarium oxysporum* f.sp *lycopersici.*

Treatment	MIC (µg/mL)	MFC (µg/mL)
Citral	512	512
Citral-loaded chitosan nanoparticles	4096	ND

Not determined- indicates no MIC or MFC. Values are means of triplicate data and, standard deviation is 0.00.

2023).

Minimum inhibitory and fungicidal concentrations (MIC & MFC)

Citral exhibited strong antifungal effectiveness with MIC and MFC values measured at 512 µg/mL. The identical MIC and MFC values for citral suggest a fungicidal effect occurring at the same concentration that initially inhibits growth, indicating that citral may act as a compound fungicide against FOL (Scorzoni et al., 2016). Previous findings, however, regarding the antifungal activity of citral against other plant fungal pathogens, depict citral as fungistatic since the MIC and MFC values are different. This difference in results could stem from fungal species variability, varying concentrations used, as well as differences in unit measurements and methodologies.

The MIC of citral-loaded chitosan nanoparticles was determined at 4096 µg/mL, while its MFC was not determined due to the range of concentrations used, as shown in Table 3. This result is consistent with the findings in the antifungal activity assay section (3.5) for mycelial growth inhibition, where citral proved more potent at lower concentrations compared to nano-encapsulated citral. The reasons for this discrepancy may be similar to those discussed previously in that section.

CONCLUSIONS AND FUTURE WORKS

This study successfully encapsulated citral within chitosan nanoparticles, as confirmed by SEM and FTIR analysis. The *in vitro* release profile also demonstrated an initial burst release followed by a slower release of citral from the nanoparticles. However, concerning antifungal activity, the mycelial growth inhibition assay revealed that pure citral exhibited significantly higher effectiveness against the pathogen than nano-encapsulated citral, even though the nanoparticles also inhibited the mycelial growth of the pathogen. The MIC and MFC values for pure citral were determined at a concentration of 512 µg/mL, suggesting that citral may serve as a potent antifungal agent against FOL. However, the MIC of the nanoparticles was

observed to be high at 4096 µg/mL, and its MFC was not determined.

Considering the findings from this study, citral in its pure form proved to be a potent antifungal agent against FOL and hence can be considered during the development of alternative fungicides against FOL. Nevertheless, further in vivo studies are essential to confirm its efficacy against this soil-borne pathogen. On the other hand, our findings indicate that the encapsulation of citral did not significantly improve its inhibitory activity. This suggests that an increase in the concentration of the nano-encapsulated citral, optimization of the encapsulation process of citral into the chitosan-tripolyphosphate system, and the addition of copolymers may improve its efficacy. Additionally, the use of different nanocarrier systems and encapsulation methods or a combination of these methods could also increase its encapsulation efficiency and subsequent antifungal activity.

CONFLICT OF INTERESTS

The authors have not declared any conflict of interests.

ACKNOWLEDGMENTS

The authors would like to express their gratitude to the African Union Commission for their generous scholarship and research funding that enabled this study. They also extend their thanks to the Institute for Biotechnology Research (IBR) at Jomo Kenyatta University of Agriculture and Technology (JKUAT) for granting access to their molecular biology lab for laboratory work. Additionally, the authors appreciate the valuable contributions made by Ifeoluwa Deborah Gbala (Trieste, Italy) to this research.

REFERENCES

Abdel-Rahman FA, Monir GA, Hassan MSS, Ahmed Y, Refaat MH, Ismail IA, El-Garhy HAS (2021). Exogenously Applied Chitosan and Chitosan Nanoparticles Improved Apple Fruit Resistance to Blue Mold, Upregulated Defense-Related Genes Expression, and Maintained Fruit Quality. Horticulturae 7(8):224.

El-Aziz AR, Al-Othman MR, Mahmoud MA, Shehata SM, Abdelazim NS (2018). Chitosan Nanoparticles as a Carrier for *Mentha longifolia* Extract: Synthesis, Characterization and Antifungal Activity. Current Science 114(10):2116-2122.

Amighi M, Zahedifar M, Alizadeh H, Payandeh M (2023). Encapsulation of Nepeta hormozganica and Nepeta dschuprensis essential oils in shrimp chitosan NPs: Enhanced antifungal activity. International Journal of Biological Macromolecules 238:124112.

Anitha A, Deepagan VG, Divya Rani VV, Menon D, Nair SV, Jayakumar R (2011). Preparation, characterization, in vitro drug release and biological studies of curcumin loaded dextran sulphate–chitosan nanoparticles. Carbohydrate Polymers 84(3):1158-1164.

Ayesha MS, Suryanarayanan TS, Nataraja KN, Prasad SR, Shaanker RU (2021). Seed Treatment with Systemic Fungicides: Time for Review. Frontiers in Plant Science 12:654512. https://doi.org/10.3389/fpls.2021.654512

Bagheri R, Ariaii P, Motamedzadegan A (2021). Characterization, antioxidant and antibacterial activities of chitosan nanoparticles loaded with nettle essential oil. Journal of Food Measurement and Characterization 15(2):1395-1402.

Bassolé IHN, Juliani HR (2012). Essential Oils in Combination and Their Antimicrobial Properties. Molecules 17(4):3989-4006.

Beatrice C, Linthorst JMH, Cinzia F, Luca R (2017). Enhancement of PR1 and PR5 gene expressions by chitosan treatment in kiwifruit plants inoculated with *Pseudomonas syringae* pv. *actinidiae*. European Journal of Plant Pathology 148(1):163-179.

Begines B, Ortiz T, Pérez-Aranda M, Martínez G, Merinero M, Argüelles-Arias F, Alcudia A (2020). Polymeric Nanoparticles for Drug Delivery: Recent Developments and Future Prospects. Nanomaterials 10(7):1403.

Bouissil S, Guérin C, Roche J, Dubessay P, Alaoui-Talibi ZE, Pierre G, Michaud P, Mouzeyar S, Delattre C, Modafar CE (2022). Induction of Defense Gene Expression and the Resistance of Date Palm to *Fusarium oxysporum* f. sp. Albedinis in Response to Alginate Extracted from Bifurcaria bifurcata. Marine Drugs 20(2):88. https://doi.org/10.3390/md20020088

Cai J, Yang D, Wang Q (2023). Preparation and characterization of chitosan nanoparticles loaded with Athyrium sinense essential oil with antibacterial properties against *Pectobacterium carotovorum* subsp. carotovorum. Industrial Crops and Products 195:116382. https://doi.org/10.1016/j.indcrop.2023.116382

Chun SC, Chandrasekaran M (2019). Chitosan and chitosan nanoparticles induced expression of pathogenesis-related proteins genes enhances biotic stress tolerance in tomato. International Journal of Biological Macromolecules 125:948-954.

Devi NO, Devi R, Debbarma M, Hajong M, Thokchom S (2022). Effect of endophytic Bacillus and arbuscular mycorrhiza fungi (AMF) against Fusarium wilt of tomato caused by *Fusarium oxysporum* f. sp. lycopersici. Egyptian Journal of Biological Pest Control 32:1-14.

Dey P, Ramanujam R, Venkatesan G, Radhakrishnan N (2019). Sodium alginate potentiates antioxidant defense and PR proteins against early blight disease caused by Alternaria solani in *Solanum lycopersicum* Linn. PLoS One 14(9):e0223216.

Hadidi M, Pouramin S, Adinepour F, Haghani S, Jafari SM (2020). Chitosan nanoparticles loaded with clove essential oil: Characterization, antioxidant and antibacterial activities. Carbohydrate Polymers 236:116075.

Haider J, Majeed H, Williams PA, Safdar W, Zhong F (2017). Formation of chitosan nanoparticles to encapsulate krill oil (*Euphausia superba*) for application as a dietary supplement. Food Hydrocolloids 63:27-34.

Hoang NH, Le Thanh T, Sangpueak R, Treekoon J, Saengchan C, Thepbandit W, Papathoti NK, Kamkaew A, Buensanteai N (2022). Chitosan Nanoparticles-Based Ionic Gelation Method: A Promising Candidate for Plant Disease Management. Polymers 14(4):662. https://doi.org/10.3390/polym14040662

Hosseini SF, Zandi M, Rezaei M, Farahmandghavi F (2013). Two-step method for encapsulation of oregano essential oil in chitosan nanoparticles: Preparation, characterization and in vitro release study. Carbohydrate Polymers 95(1):50-56.

Jia L, Wang R, Fan Y (2020). Encapsulation and release of drug nanoparticles in functional polymeric vesicles. Soft Matter 16(12):3088-3095.

Jian W, Khelissa S, Chihib N, Dumas É, Gharsallaoui A. (2019). Effect of drying and interfacial membrane composition on the antimicrobial activity of emulsified citral. Food Chemistry 298:125079. https://doi.org/10.1016/j.foodchem.2019.125079

Kalagatur NK, Nirmal Ghosh OS, Sundararaj N, Mudili V (2018). Antifungal Activity of Chitosan Nanoparticles Encapsulated with *Cymbopogon martinii* Essential Oil on Plant Pathogenic Fungi *Fusarium graminearum*. Frontiers in Pharmacology 9:610. https://doi.org/10.3389/fphar.2018.00610

Kalleli F, Abid G, Salem IB, Boughalleb-M'Hamdi N, Mahmoud MA (2020). Essential oil from fennel seeds (Foeniculum vulgare) reduces Fusarium wilt of tomato (*Solanum lycopersicon*). (DOAJ: Directory of Open Access Journals). https://doi.org/10.14601/phyto-11143

Kaur G, Ganjewala D, Bist V, Verma PC (2019). Antifungal and larvicidal activities of two acyclic monoterpenes; citral and geraniol

against phytopathogenic fungi and insects. Archives of Phytopathology and Plant Protection 52(5-6):458-469.
Keawchaoon L, Yoksan R (2011). Preparation, characterization and in vitro release study of carvacrol-loaded chitosan nanoparticles. Colloids and surfaces B: Biointerfaces 84(1):163-171.
Khanmohammadi M, Elmizadeh H, Ghasemi K (2015). Investigation of size and morphology of chitosan nanoparticles used in drug delivery system employing chemometric technique. PubMed 14(3):665-675.
Kiirika LM, Stahl F, Wydra K (2013). Phenotypic and molecular characterization of resistance induction by single and combined application of chitosan and silicon in tomato against *Ralstonia solanacearum*. Physiological and Molecular Plant Pathology 81:1-12.
La Torre A, Caradonia F, Matere A, Battaglia V (2016). Using plant essential oils to control Fusarium wilt in tomato plants. European Journal of Plant Pathology 144(3):487-496.
Lammari N, Louaer O, Meniai AH, Elaissari A (2020). Encapsulation of Essential Oils via Nanoprecipitation Process: Overview, Progress, Challenges and Prospects. Pharmaceutics 12(5):431.
Li J, Zhou X, Zhang C, Zhao Y, Zhu Y, Zhang J, Bai J, Xiao X (2020). The Effects of Carbendazim on Acute Toxicity, Development, and Reproduction in *Caenorhabditis elegans*. Journal of Food Quality 2020:1-6.
Linde JH, Combrinck S, Regnier TJC, Virijevic S (2010). Chemical composition and antifungal activity of the essential oils of *Lippia rehmannii* from South Africa. South African Journal of Botany 76(1):37-42.
Liu G, An D, Li J, Deng S (2023). Zein-based nanoparticles: Preparation, characterization, and pharmaceutical application. Frontiers in Pharmacology 14:1120251.
Lü W, Huang DW, Wang CC, Yeh C, Tsai JC, Huang Y, Li PH (2018). Preparation, characterization, and antimicrobial activity of nanoemulsions incorporating citral essential oil. Journal of Food and Drug Analysis 26(1):82-89.
Ma H, Zhao Y, Lu Z, Xing R, Yao X, Jin Z, Wang Y, Yu F (2020). Citral-loaded chitosan/carboxymethyl cellulose copolymer hydrogel microspheres with improved antimicrobial effects for plant protection. International Journal of Biological Macromolecules 164:986-993.
Marei GIK, Rabea EI, Badawy ME (2018). Preparation and Characterizations of Chitosan/Citral Nanoemulsions and their Antimicrobial Activity. (DOAJ: Directory of Open Access Journals). https://doi.org/10.22037/afb.v5i2.19005
Maswal M, Dar AA (2014). Formulation challenges in encapsulation and delivery of citral for improved food quality. Food Hydrocolloids 37:182-195.
Nagpal K, Singh SK, Mishra DN (2010). Chitosan nanoparticles: a promising system in novel drug delivery. Chemical and Pharmaceutical Bulletin 58(11):1423-1430.
Nunes MR, Agostinetto L, Da Rosa CG, Sganzerla WG, Pires MF, Munaretto GA, Rosar CR, Bertoldi FC, Barreto PLM, De Lima Veeck AP, Zinger FD (2024). Application of nanoparticles entrapped orange essential oil to inhibit the incidence of phytopathogenic fungi during storage of agroecological maize seeds. Food Research International 175:113738. https://doi.org/10.1016/j.foodres.2023.113738
Oleandro E, Stanzione M, Buonocore GG, Lavorgna M (2024). Zein-Based nanoparticles as active platforms for Sustainable applications: recent advances and perspectives. Nanomaterials 14(5):414. https://doi.org/10.3390/nano14050414
Oluoch G, Matiru V, Mamati EG, Nyongesa M (2021). Nanoencapsulation of Thymol and Eugenol with Chitosan Nanoparticles and the Effect against *Ralstonia solanacearum*. Advances in Microbiology 11(12):723-739.
Rasteh I, Pirnia M, Miri MA, Sarani S (2024). Encapsulation of *Zataria multiflora* essential oil in electrosprayed zein microcapsules: Characterization and antimicrobial properties. Industrial Crops and Products 208:117794. https://doi.org/10.1016/j.indcrop.2023.117794
Santos CMD, De Araújo Gonçalves M, De Macedo LF, Torres AHF, Marena GD, Chorilli M, Trovatti E (2023). Green nanotechnology for the development of nanoparticles based on alginate associated with essential and vegetable oils for application in fruits and seeds protection. International Journal of Biological Macromolecules 232:123351. https://doi.org/10.1016/j.ijbiomac.2023.123351
Scorzoni L, Sangalli-Leite F, De Lacorte Singulani J, De Paula E Silva ACA, Costa-Orlandi CB, Fusco-Almeida AM, Mendes-Giannini MJS (2016). Searching new antifungals: The use of *in vitro* and *in vivo* methods for evaluation of natural compounds. Journal of Microbiological Methods 123:68-78.
Servat-Medina L, González-Gómez A, Reyes-Ortega F, Sousa IMO, Queiroz NDCA, Zago PMW, Jorge MP, Monteiro KM, Carvalho JE, San Román J, Foglio MA (2015). Chitosan tripolyphosphate nanoparticles as *Arrabidaea chica* standardized extract carrier: Synthesis, characterization, biocompatibility, and antiulcerogenic activity. International Journal of Nanomedicine pp. 3897-3909.
Sharma A, Harjai K, Ramniwas S, Singh D (2023). Bioactivity of Citral and Its Nanoparticle in Attenuating Pathogenicity of *Pseudomonas aeruginosa* and Controlling *Drosophila melanogaster*. Journal of Nanomaterials 2023:1-11.
Sharma A, Rajendran S, Srivastava A, Sharma S, Kundu B (2017). Antifungal activities of selected essential oils against *Fusarium oxysporum* f. Sp. *lycopersici* 1322, with emphasis on *Syzygium aromaticum* essential oil. Journal of Bioscience and Bioengineering 123(3):308-313.
Shetta A, Kegere J, Mamdouh W (2019). Comparative study of encapsulated peppermint and green tea essential oils in chitosan nanoparticles: Encapsulation, thermal stability, in-vitro release, antioxidant and antibacterial activities. International Journal of Biological Macromolecules 126:731-742.
Srinivas C, Devi D, Murthy KN, Mohan CD, Lakshmeesha TR, Singh BP, Kalagatur NK, Niranjana SR, Hashem A, Tabassum B, Nayaka SC (2019). *Fusarium oxysporum* f. sp. *lycopersici* causal agent of vascular wilt disease of tomato: Biology to diversity– A review. Saudi Journal of Biological Sciences 26(7):1315-1324.
Tian H, Lu Z, Li D, Hu J (2018). Preparation and characterization of citral-loaded solid lipid nanoparticles. Food Chemistry 248:78-85.
Wei L, Chen C, Chen J, Lin L, Wan C (2021). Possible fungicidal effect of citral on kiwifruit pathogens and their mechanisms of actions. Physiological and Molecular Plant Pathology 114:101631. https://doi.org/10.1016/j.pmpp.2021.101631
Worrall E, Hamid A, Mody K, Mitter N, Pappu H (2018). Nanotechnology for Plant Disease Management. Agronomy 8(12):285. https://doi.org/10.3390/agronomy8120285
Xing K, Zhu X, Peng X, Qin S (2015). Chitosan antimicrobial and eliciting properties for pest control in agriculture: A review. Agronomy for Sustainable Development 35(2):569-588.
Yammine J, Chihib N, Gharsallaoui A, Ismail A, Karam L (2023). Advances in essential oils encapsulation: development, characterization and release mechanisms. Polymer Bulletin 81(5):3837-3882.
Yang L, Wen KS, Ruan X, Zhao YX, Wei F, Wang Q (2018). Response of Plant Secondary Metabolites to Environmental Factors. Molecules 23(4):762. https://doi.org/10.3390/molecules23040762
Yassin MT, Mostafa AAF, Al-Askar AA (2021). *In vitro* antagonistic activity of *Trichoderma harzianum* and *T. viride* strains compared to carbendazim fungicide against the fungal phytopathogens of *Sorghum bicolor* (L.) Moench. Egyptian Journal of Biological Pest Control 31(1):118. https://doi.org/10.1186/s41938-021-00463-w
Zhao X, Zhang Y, Chen L, Ma Z, Zhang B (2023). Chitosan-thymol nanoparticle with pH responsiveness as a potential intelligent botanical fungicide against *Botrytis cinerea*. Pesticide Biochemistry and Physiology 195:105571. https://doi.org/10.1016/j.pestbp.2023.105571
Zhu G, Feng N, Xiao Z, Zhou R, Niu Y (2015). Production and pyrolysis characteristics of citral–monochlorotriazinyl-β-cyclodextrin inclusion complex. Journal of Thermal Analysis and Calorimetry 120(3):1811-1817.

Vol. 23(4), pp.142-146, April 2024
DOI: 10.5897/AJB2023.17627
Article Number: 0B1BBCF72058
ISSN: 1684-5315

http://www.academicjournals.org/AJB

ACADEMIC JOURNALS
expand your knowledge

African Journal of Biotechnology

Full Length Research Paper

Isolation and binary fusion of taro (*Colocasia esculeneta* (L) Schott.) protoplast: Towards developing somatic hybridization protocol as an alternative to sexual hybridization

Mohamed Chungwa[1]*, Robert Gesimba[1] and Abwao S. Indieka[2]

[1]Crops, Horticulture and Soils Department, Egerton University, P. O. Box 536-20115 Egerton, Njoro, Kenya.
[2]Biochemistry and Molecular Biology Department, Egerton University, P. O. Box 536-20115 Egerton, Njoro, Kenya.

Received 7 November, 2023; Accepted 12 December, 2023

***Collocasia esculenta* (L) Schott. (Taro) genotypes cultivated in Kenya rarely produce flowers, thus improvement via pollination is hindered. Somatic hybridization is an attractive alternative to circumvent flower pollination constrain and hence explored in this study. The aim of this study was to optimize isolation and binary fusion of protoplast obtained from *C. esculenta* (Dasheen) and *C. antiquorum* Eddoe) genotypes. Protoplast was isolated from embryogenic calli and leaf tissues using cellulase R-10 (1.0% w/v) combined with pectinase R-10 (0.15% w/v). Fusion of leaf- and calli-derived protoplast was conducted using PEG 6000 (0-30% w/v), $CaCl_2$ (0-0.15 M) and $NaNO_3$ (0-4% w/v). Overall, 2 to 4 h enzyme incubation and PEG (10 or 20%) treatments for 10 to 20 min, were optimal for isolation of viable protoplast and fusion, respectively. The capacity of binary fusions to form cell colonies was higher when fusion was undertaken using PEG at either 10 or 20% after 10 and 20 min incubation. The study demonstrates that optimized protoplast fusion is a viable alternative for taro improvement that by passes flowering constrain.**

Key words: Taro, protoplast, binary fusion, somatic hybridization, PEG 6000, heterokarya.

INTRODUCTION

Taro (*Colocasia esculenta* and *Colocasia antiquorum* L. Schott) is an important staple root crop in Asia, Pacific Islands, and sub-Saharan Africa (SSA) (Chaïr et al., 2016; Grimaldi and van Andel, 2018; Oladimeji et al., 2022). It belongs to family Araceae that comprises at least 100 genera and more than 1500 species (Henriquez et al., 2014). In eastern Africa, taro is cultivated for its edible corms, with production estimated at 2,998,780

*Corresponding author. E-mail: 2898859469@qq.com

tons in the year 2020 (FAOSTAT, 2021). Taro landrace and cultivars grown in Kenya rarely flower, therefore, development of new varieties or improvement of existing cultivars through pollination is difficult. Dasheen type, locally known as Nduma ngirigacha is the widely cultivated variety in Kenya, though introduced by the colonial government in the 1940s. In addition, three indigenous Dasheen cultivars are either rarely cultivated or grow wildly. These Dasheen cultivars are less popular due to poor yield and high acridity levels (Grimaldi and van Andel, 2018). Indigenous Eddoe type, locally known as Nduma mwanake, grows wildly on farm periphery in central Kenya region (Grimaldi and van Andel, 2018). Despite wider applications of *in vitro* cell culture techniques, there are no reports on protoplast isolation, culture and fusion for taro cultivars from SSA, unlike for pacific and Asia (Verma and Cho, 2010).

Natural hybridization constraints such as parental or genotype incompatibility and flowering difficulty can be addressed via inter specific and inter generic protoplast fusion (Millam et al., 1995; Ranaware et al., 2023). This is because there are few barriers to protoplast fusion and therefore gene transfer can be achieved despite natural hybridization constraints. Somatic hybrids plants are regenerated through embryogenesis or organogenesis. Plant protoplast fusion has successfully been used to transfer disease resistance and other qualitative traits (Dutt et al., 2021). Indeed, availability of reproducible protoplast isolation, fusion and plant regeneration protocols will open new opportunities for developing new or improving SSA taro cultivars. However, protocol development is highly influenced by genotype, donor tissue, enzyme combination, culture media, and physiological status of the cells among others (Reed and Bargmann, 2021; Ranaware et al., 2023). This necessitates optimization or development of suitable protocol for each plant genotype. Therefore, the aim of the study was to optimize isolation and binary fusion of leaf- and calli-derived protoplast obtained from *C. esculenta* (Dasheen) and *C. antiquorum* (Eddoe) genotypes.

MATERIALS AND METHODS

Plant

In vitro stock plants were established using taro cultivar Ngirigacha (Dasheen) and Nduma mwanake (Eddoe) explants collected from farms in Kiambu and Meru counties in Central Kenya Region. Leaf explants were obtained from *in vitro* grown *C. esculenta* and *C. antiquorum* stock plants. On the other hand, embryogenic calli was generated using microcorm (ca. 0.5 mm) slices obtained from *in vitro* stock plants and 1/2 Murashige and Skoog (MS) + 4 mg/L 2,4-Dichlorophenoxyacetic acid (2, 4-D) + 0.5 thidiazuron (TDZ). However, optimal induction of embryogenic calli was first determined using micro-corm explants cultured on semi solid 1/2 MS media containing 2, 4-D (1, 2 and 4 mg/L) alone or combined with TDZ (0.5 or 1 mg/L) in dark at 27°C for 30 days. Embryogenic calli were excised from explants and sub-cultured on respective induction media for 30 days. Media pH was adjusted to 5.8 and was supplemented with sucrose (30 g/L) and gelrite (3 g/L). The number of explants forming calli, type of calli, size of calli and quality proliferating of calli after subculture were assessed.

Protoplast isolation from leaf and embryogenic calli tissues

Protoplast was isolated from leaf and embryogenic calli tissues. Leaves were obtained from *in vitro* grown *C. esculenta* and *C. antiquorum*, while microcorm-embryogenic calli were induced using 1/2 MS+ 2 mg/L 2,4-D + 0.5 mg/L TDZ media. Sliced leaf (ca. 3-4 mm^2) and calli tissues were incubated in dark at 26°C for 1, 2, 4 and 6 h in 5 mL in enzyme cocktail consisting of 0.5% w/v pectinase and 1% w/v cellulose. At the end of each incubation period, tissues-enzyme mixtures were transferred to a sterile nylon mesh (75 µm), then washed using 15% sucrose, pH 5.8 (washing medium). The filtrates were centrifuged at 100 rpm for 5 min, pellets re-suspended in 5 mL washing medium and protoplast fractions recovered using Pasteur pipette. Viable protoplasts for each taro type, explant type, and incubation period were evaluated using the Evan's blue method. The viable protoplasts were adjusted to 4.5×10^6 protoplast/mL.

Screening of chemical fusogens

Fusogens, (i) Polyethylene glycol (PEG) 6000 at 0, 10, 20 and 30% w/v, (ii) $CaCl_2$ at 0, 0.05, 0.1 and 0.15 M, and (iii) $NaNO_3$ at 0, 1, 2 and 4% w/v were screened. PEG and $NaNO_3$ fusogen solutions were supplemented with 0.8 M mannitol and 0.2 M 2-(N-morpholino) ethanesulfonic acid (MES), respectively, while $CaCl_2$ contained 0.4% glycine and 0.8 M mannitol and pH adjusted to 5.8. For fusion, equal volume (200 µL) of leaf and calli protoplast was mixed and then 300 µl of fusogen solutions added dropwise with gentle agitation. Protoplast-fusogen mixtures were incubated at room temperature for 10, 20 and 30 min. Aliquots (50 µL) of fusion products were observed under a microscope (×1000) and occurrence of binary fusions expressed as percentages. Binary fusion products were centrifuged at 500 rpm for 5 min and, pellet re-suspended in 1 mL 1/2 MS+ 2 mg/L 2,4-D + 0.5 mg/L TDZ + 100 mg/L glutamine and transferred into cell culture microplates. The plates were incubated with gentle agitation for 45 days in dark at 25°C to allow formation of micro-calli.

Experimental design and data analysis

All the experiments conducted were laid out in Completely Randomized Design (CRD). For induction of embryogenic calli, the effects of 2, 4-D alone or combined with TDZ were conducted separately as 2×2×3 and 2×2×6 factorial experiments. Three independent replicate experiments were conducted with 15 to 20 explants per treatment. Protoplast isolation and fusion experiments were conducted as 2×2×4 and 3×4 factorial experiments, respectively with 3 replicates per treatment. Data on number of explants forming calli was subjected to square root transformation, while percentage viable protoplast and binary fusion frequencies were transformed using arcsine prior to ANOVA ($p<0.05$) using PROC GLM code of SAS (Version 9.1). The means of treatments were separated using Tukey's Honestly Significant Difference Test ($p<0.05$).

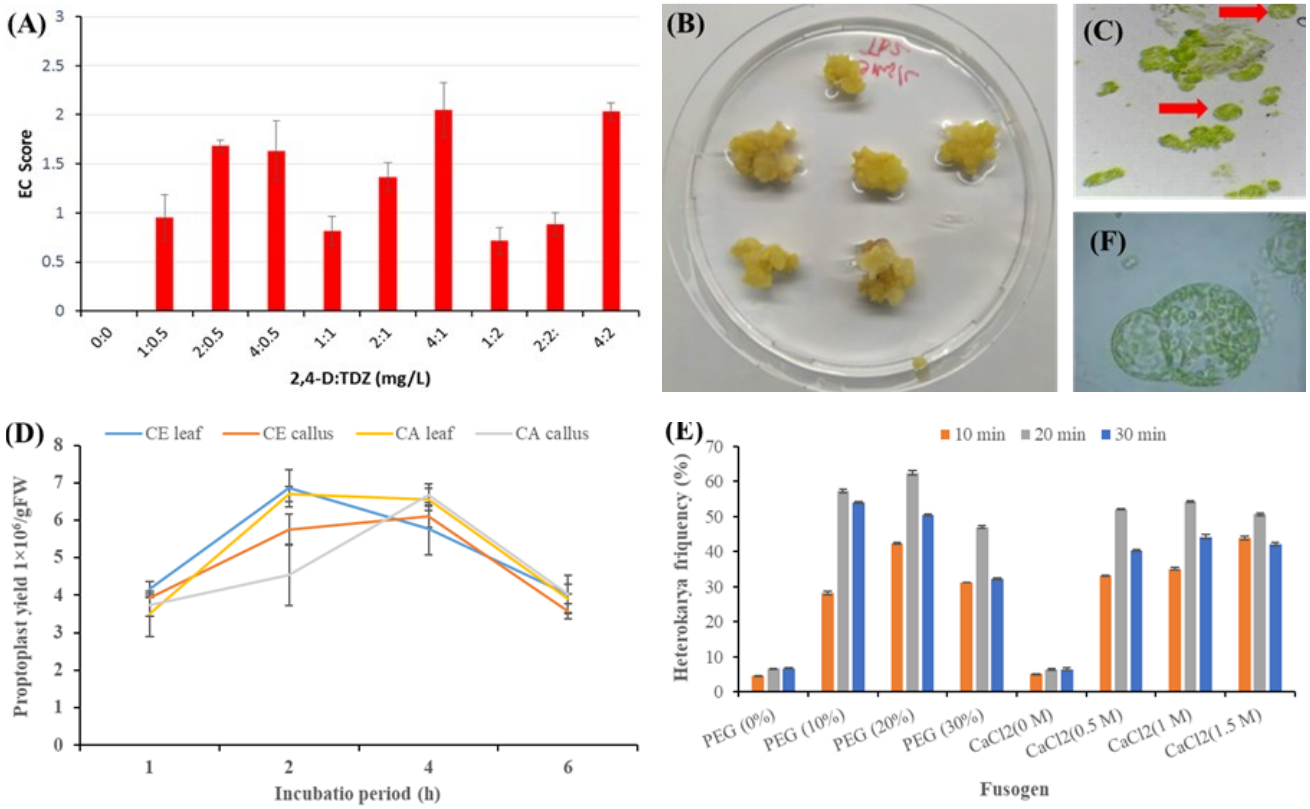

Figure 1. Induction of embryogenic calli, protoplast isolation and binary fusion of leaf- and embryogenic calli-derived protoplast obtained from taro genotypes *Collocasia esculenta* (CE) and *Collocasia esculenta antiquorum* (CA). (A) Quality of embryogenic calli on 1/2 MS media containing different combination of 2, 4-D and TDZ; (B) Proliferation of embryogenic calli on 1/2 MS+ 2, 4-D (4 mg/L) + TDZ (1.0 mg/L) at 30 days after subculture; (C) Protoplast isolated from leaf tissue with red arrow indicating intact protoplast (×1000); (D) Influence of taro genotype, tissue type and enzyme incubation period on protoplast isolation; (E). Determination of best fusogen type and optimal concentration for binary fusion (leaf and calli) of taro protoplast. Graphs are based on the means of 3 independent replicate experiments. Bars on the graphs represent standard error of mean (SEM).

RESULTS

Generally, higher numbers of micro-corm explants from *C. esculenta* and *C. antiquorum* with embryogenic calli were obtained on 1/2 MS media containing 2, 4-D (2 mg/L) combined with TDZ (0.5 mg/L) and 2, 4-D (4 mg/L) combined with TDZ either at 0.5, 1.0 or 2.0 mg/L, unlike 2, 4-D alone, which induced non embrygenic calli. A similar trend was observed on the quality of embryogenic calli induced (Figure 1A). Embryogenic calli exercised from explants proliferated well when sub-cultured on 4 mg/L 2, 4-D + 0.5 or 1 mg/L TDZ (Figure 1B). Leaf and calli derived protoplasts were green (Figure 1C) and transparent to light green in color, respectively. Incomplete release of protoplast from cell walls was observed in all incubation periods. Nonetheless, protoplast yield was influenced ($p<0.05$) by enzyme incubation period and interaction (incubation period × explant tissue). Irrespective of explant type, high numbers of viable protoplast were obtained after 2 and 4 h incubation, for leaf and calli tissues, respectively. However, further incubation > 4 h resulted in yield reduction (Figure 1D). Overall, highest protoplast yield was obtained on leaf explants regardless of taro genotype (Figure 1D). Fusogen concentration, incubation period and interaction (fusogen × incubation) significantly ($p<0.05$) influenced binary fusion frequencies. Regardless of incubation period and concentration, lower (≤33 %) binary fusion frequencies were obtained using $NaNO_3$. On the other hand, 20 min incubation in PEG and $CaCl_2$ across the concentrations tested produced higher binary frequencies, while >20 min incubation reduced fusion frequencies (Figure 1E). Overall, PEG at 20% produced significantly ($p<0.05$) higher (62.5%) number of heterokarya after 20 min incubation (Figure 1E). Majority of the heterokarya observed consisted of leaf- and calli-protoplast fusion. However, fusion of two protoplasts from the same tissue (Figure 1F) and multi-fusions were also

observed. The capacity of binary fusions to form cell colonies was higher when fusion was undertaken using PEG at 10 or 20% after 10 or 20 min incubation.

DISCUSSION

In vitro plant regeneration is influenced by a number of factors; however, for induction of somatic embryos, the key factors are plant growth regulators (PGRs) type, explant type, genotype, and culture conditions (Deo et al., 2010). The results obtained using corm explants from *C. esculenta* and *C. antiquorum*s suggest that genotype was not a major factor that influenced induction of embryogenic calli. Nonetheless, the results demonstrate that PGRs concentration, type and combination had a major influence induction of taro embryogenic calli. These results are in line with studies conducted using Asia Pacific taro genotypes (Deo et al., 2009). Decline in viable protoplast frequency associated with enzyme incubation >4 h for both leaf and calli tissues was not expected. This is because prolonged enzyme incubation is supposed to ensure greater explant penetration and hence increased protoplast yields (Davey et al., 2005). However, the results suggest that prolonged enzyme exposure compromise the integrity of viable protoplasts. Furthermore, protoplast isolation mimics wounding stress in plants and thus enzyme exposure >4 h might have led to acidification of cytosol due to accumulation of oligo-galacto lipids that led to disintegration of isolated protoplasts (Barnes et al., 2019). Therefore, isolation of taro protoplast from leaf and calli tissues was optimal within 2 to 4 h incubation. Despite higher yields obtained from leaf tissues, both explant type and taro genotype influenced viable protoplast yield. The genotype effect on taro protoplast yields has been reported and was ascribed to varied release of compounds from chopped leaves that inhibited enzymatic cell wall digestion (Reed and Bargmann, 2021). Fusogens reduce plasma membrane negative charges; hence, allowing protoplasts to fuse (Ahmed et al., 2021). Therefore, variations in binary fusion frequencies can be attributed to varied effects of fusogen types and concentrations on reducing negative plasma membrane charges. On the other hand, the inverse relationship between binary fusion frequencies and fusogen concentrations obtained, clearly demonstrate that prolonged exposure and higher fusogen concentration did not favor fusion of taro protoplast.

Conclusion

Induction of friable embryogenic calli using micro corm explant was optimal when 24-D (2-4 mg/L) was combined with TDZ (0.5 mg/L). Whereas, 2 to 4 h incubation of leaf and embryogenic calli tissues in cellulase R-10 (1.0% w/v) combined with pectinase R-10 (0.15% w/v) was sufficient for isolation of viable protoplast. On the other hand, PEG (10 or 20%) was optimal for fusing leaf and embryogenic calli protoplast. Protoplast isolation and fusion protocol described in the study provides a simple procedure that ensures satisfactory yields, quick recovery of viable protoplasts, and heterokarya. Protoplast survival and division after fusion ascertained the competence of the protoplasts isolated. However, further research to determine optimal media formulation for culturing taro heterokarya and subsequent plant regeneration is required. The study demonstrates that optimized protoplast fusion coupled with plant regeneration is a viable alternative to natural hybridization of taro via cross-pollination.

CONFLICT OF INTERESTS

The authors have not declared any conflict of interests.

ACKNOWLEDGEMENTS

This study was supported by funding from Nation Research Fund-Kenya (NRF-K) through a Research Grant (NRF/1/MMC/163) awarded to A. S. Indieka, CESAAM Egerton University Scholarship to Mohamed Chungwa and The Belt and Road Molecular Laboratory at Egerton University, where experiments were conducted.

REFERENCES

Ahmed MAA, Miao M, Pratsinakis ED, Zhang H, Wang W, Yuan Y, Lyu M, Iftikhar J, Yousef AF, Madesis P, Wu B (2021). Protoplast isolation, fusion, culture and transformation in the woody plant *Jasminum* spp. Agriculture 11(8):699-719.

Barnes AC, Elowsky CG, Roston RL (2019). An Arabidopsis protoplast isolation method reduces cytosolic acidification and activation of the chloroplast stress sensor sensitive to freezing 2. Plant Signaling and Behavior 14(9):1-9.

Chaïr H, Traore RE, Duval MF, Rivallan R, Mukherjee A, Aboagye LM, Van Rensburg WJ, Andrianavalona, V, Pinheiro de Carvalho MAA, Saborio F, Prana MS, Komolong B, Lawac F, Lebot V (2016). Genetic diversification and dispersal of taro (*Colocasia esculenta* (L.) schott). PLoS One 11(6):e0157712.

Davey MR, Anthony P, Power JB, Lowe KC (2005). Plant protoplasts: status and biotechnological perspectives. Biotechnology Advances 23:131-171.

Deo PC, Harding RM, Taylor M, Tyagi AP, Becker DK (2009). Somatic embryogenesis, organogenesis and plant regeneration in taro (*Colocasia esculenta* var. *esculenta*). Plant Cell Tissue and Organ Culture 99:61-71.

Deo PC, Tyagi AP, Taylor M, Harding R, Becker D (2010). Factors affecting somatic embryogenesis and transformation in modern plant breeding. The South Pacific Journal of Natural and Applied Sciences 28(1):27-40.

Dutt M, Mahmoud LM, Chamusco K, Stanton D, Chase CD, Nielsen E, Quirico M, Yu Q, Gmitter FG, Grosser JW (2021). Utilization of somatic fusion techniques for the development of HLB tolerant breeding resources employing the Australian finger lime (*Citrus australasica*). PLoS One 16(8):e0255842.

FAOSTAT (2021). Food and Agriculture Organization [WWW Document]. FAOSTAT. Available at: https://www.fao.org/faostat/en/#data/QCL

Grimaldi IM, van Andel TR (2018). Food and medicine by what name? Ethnobotanical and linguistic diversity of taro in Africa. Economic Botany 72:217-228.

Henriquez CL, Arias T, Pires JC, Croat TB, Schaal BA (2014). Phylogenomics of the plant family Araceae. Molecular Phylogenetics and Evolution 75:91-102.

Millam S, Payne LA, Mackay GR (1995). The integration of protoplast fusion-derived material into a potato breeding programme: a review of progress and problems. Euphytica 85:451-455.

Oladimeji JJ, Kumar PL, Abe A, Vetukuri RR, Bhattacharjee R (2022). Taro in West Africa: status, challenges, and opportunities. Agronomy 12(9):2094.

Reed KM, Bargmann BOR (2021). Protoplast regeneration and its use in new plant breeding technologies. Frontiers in Genome Editing 3:734951.

Verma VM, Cho JJ (2010). Plantlet development through somatic embryogenesis and organogenesis in plant cell cultures of *Colocasia esculenta* (L.) schott. Asia Pacific Journal of Molecular Biology and Biotechnology 18:165-168.

Ranaware AS, Kunchge NS, Lele SS, Ochatt SJ (2023). Protoplast Technology and Somatic Hybridisation in the Family Apiaceae. Plants 12(5):1060.

Vol. 23(4), pp.147-151, April 2024
DOI: 10.5897/AJB2024.17664
Article Number: 2E9473372081
ISSN: 1684-5315

http://www.academicjournals.org/AJB

ACADEMIC JOURNALS
expand your knowledge

African Journal of Biotechnology

Full Length Research Paper

Evaluation of the seroprevalence of okra mosaic virus in Koulikoro, Mali

Gaoussou K. KEITA[1], Laya KANSAYE[1], Lassina DOUMBIA[2]*, Boubacar MACALOU[2], Ibrahim KEITA[2], Mariam SANGARE[2], Moussa Noussourou MAIGA[3], Nadou Paul SANOGO[1] and Ousmane KOITA[2]

[1]Institut Polytechnique Rural de Formation et de Recherche Appliquée (IPR/IFRA), Katibougou, Koulikoro, Mali.
[2]Laboratoire de Biologie Moléculaire Appliquée (LBMA), Université des Sciences, des Techniques et des Technologies de Bamako (USTTB), Bamako, Mali.
[3]Institut Economie Rural, Bamako, Mali.

Received 12 March, 2024; Accepted 11 April, 2024

Mosaic virus disease is transmitted by several types of viruses such as OMD, OYVMV, OLCV, CLCuGV, and CYCrV. Among these viruses, some of them are significant threats to okra production worldwide. To develop an integrated pest management strategy against this disease, this seroprevalence study was conducted at the Rural Polytechnic Institute (RPI) of Katibougou, Koulikoro region, Mali. Symptomatic leaves of okra plants were collected in Koulikoro. The symptoms were mosaic associated or not with other symptoms. For this purpose, 52 symptomatic samples and 3 asymptomatic samples collected in the villages of Niarébougou, RPI Katibougou, and Diakitébougou were analyzed. The DAS ELIZA Okra Mosaic Virus (OkMV) kit was used. Among the symptomatic samples, the analyses showed the presence of 13 positive samples. This indicates a prevalence of 25% in the study area. Okra is infected by the okra virus disease called Okra Mosaic Virus (OkMV), which is the first time in Mali to be detected by the ELIZA test. This study shows the prevalence of the okra mosaic virus in Mali and more precisely in Koulikoro. This study shows the importance of keeping OKMV in consideration among the threats to okra cultivation in this area.

Key words: Seroprevalence, okra mosaic virus, Mali.

INTRODUCTION

Okra, *Abelmochus esculentus*, is a tropical plant native to Africa. It is cultivated for its nutrient richness and importance in the diet of urban and rural populations (Khomsug et al., 2010). Okra does not require significant processing before consumption, the fruits are generally sold fresh, sometimes dried into a powder (Ouoba et al., 2010).

These young leaves and fruits are edible as a sauce in most West African countries. The fruit contains many nutrients (calcium, iron, carbohydrates, proteins, vitamins, etc.) that are necessary supplements to the basic diet consisting mainly of starch (cereals and tubers) among African populations.

The economic importance of okra, its diverse uses, and

*Corresponding author. E-mail: dolslassina@yahoo.fr.

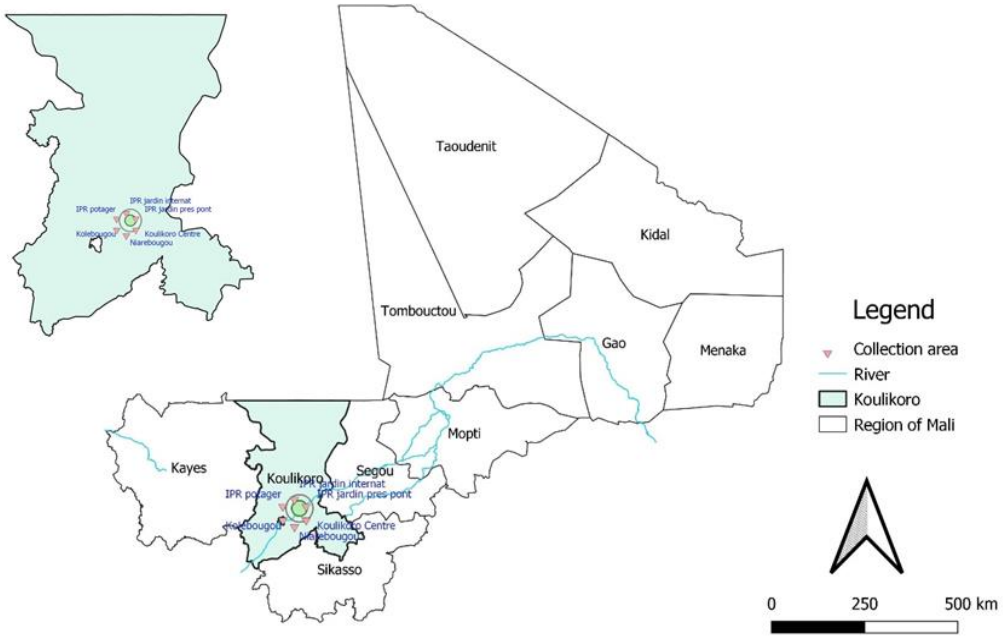

Figure 1. Okra sample collection site.

its nutritional value in the diet of the population make this crop a real tool for poverty alleviation in rural, urban, and peri-urban areas (Fondio et al., 2011). Unfortunately, this crop is confronted with the harmful action of several diseases and pests. These diseases can be of several types: viral (mosaic, leaf curl) and fungal (Cercosporiosis, fusariosis) (Ugwoke and Onyishi, 2009). In West Africa, okra mosaic virus is widespread and is usually transmitted by insect vectors (Givord and Hirth, 1973; Asare-Bediako et al., 2017). Vector control, therefore, seems to be an effective means of prevention. Chemical control of these insect vectors is widely used but the resulting intensive use of insecticides has a heavy environmental impact (Asare-Bediako et al., 2014a). Because of these undesirable effects, it is necessary to seek effective control methods that respect human and environmental health, such as farming techniques of crop associations (Kadri et al., 2013). Okra mosaic virus disease is manifested according to okra species, leaves may be covered with a coarse chlorotic mosaic or a band of veins and a pale green or yellow mosaic or irregular chlorotic areas (Givord and Hirth, 1973; Givord, 1977). Symptoms also vary according to growth stage, on the first diseased leaves a few days (7-8) after infection, they may show a green or yellow mosaic or chlorosis of the regular veins, and on the second and third diseased leaves, one to three of the central veins may be bordered by wide chlorotic bands of variable width. More rarely, symptoms are a mixture of dark green and light or whitish areas of irregular shape on the lamella (Givord and Hirth, 1973; Givord, 1977). This study aimed to search for these symptoms in Koulikoro, Mali, and to estimate the disease seroprevalence.

MATERIALS AND METHODS

Study location

This is a cross-sectional study. Okra leaf samples were collected in Koulikoro, Mali's second administrative region, during the year 2020. The study area has a Sudano-Sahelian climate characterized by a short rainy season of 4 to 5 months (late June to September) and a long dry season of 8 to 9 months (October to June). Annual rainfall is low at the beginning and reaches its maximum in August (600 to 900 mm).

Sampling involved young leaves with symptoms resembling those caused by okra viruses. Symptoms sought on the leaves were: mosaics, discoloration, waffling and rolling.

Samples were collected in the Koulikoro region, specifically in the vegetable garden, the boarding school garden, near the bridge and Diakitébougou (at the RPI), Niarébougou and the center of Koulikoro (Figure 1). A total of three non-symptomatic samples were collected. The collection of symptomatic samples was done during the pre-wintering and post-wintering period. Also, three young asymptomatic leaves samples were collected to serve as a control. One sample consisted of a diseased plant. The samples collected were labeled according to the place of collection and were then transported at 4°C to the Laboratory of Applied Molecular Biology (LBMA) in Bamako within the same week. Samples were stored in a freezer at -80°C until analysis.

Serological detection

Identification of Okra Mosaic Virus (OkMV) in the collected okra leaf samples was done by a Double Antibody Sandwich - Enzyme Linked Immuno Sorbent Assay (DAS-ELISA). The test was conducted according to the manufacturer's instructions (ACD, Inc.,

Table 1. Characteristics of okra leaves samples collected.

Site	Symptoms			Total number
	Leafroll + Mosaic	Leafroll + Mosaic + Yellow spots	Leafroll mosaic + Waffling	
RPI Diakitebougou	2	0	0	**2**
RPI boarding garden	0	1	0	1
RPI garden near bridge	2	0	0	2
RPI garden	6	0	0	6
Kolebougou	15	0	0	15
Koulikoro Downtown	5	0	0	5
Niarebougou	0	0	21	21
Total number	30	1	21	52

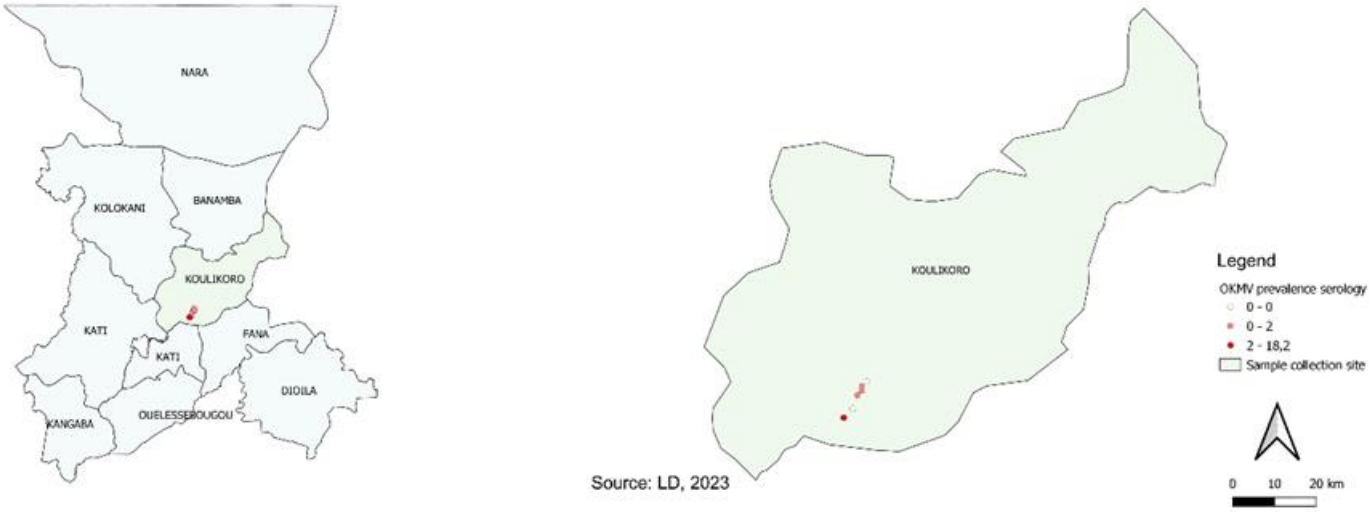

Figure 2. Distribution of Okra Mosaic Virus seroprevalence in the collection site.

Nano Diagnostics, LLC, Fayetteville, USA; https://www.nanodiaincs.com).

Reading of positive or negative reactions was done using an automated 405 nm ELISA plate reader (Biotek ELx808).

Test results were validated only if the positive control wells gave a positive result (yellow staining) and the negative control wells remained clear.

Data entry and analysis

The data were recorded in a logbook, the results obtained after the serological analysis were entered in an Excel file. Data analysis was done using R software. Mapping was done using QGIS software version 3.16.3-Hannover.

RESULTS AND DISCUSSION

Characteristics of collected samples

The study was carried out in the Koulikoro region, which is an agricultural and market gardening area per excellence. Table 1 presents the symptoms observed and the number of samples collected; a total of 52 symptomatic samples and 3 non-symptomatic samples. Symptoms encountered during this study were: mosaic-associated or not, leafroll plus yellow spot (RPI, boarding garden), leafroll plus waffling (Niarebougou), and leafroll alone in the other collection sites.

It was found that mosaic was most often associated with other symptoms in this study. This finding was reported by Konaté et al. (1995) in their study. Waffling and curling symptoms generally cause much more losses (N'Guessan et al., 1992; Kumar et al., 2010; Tiendrébéogo et al., 2010; Haruna and Jabil, 2017).

The study found an overall okra mosaic virus (OkMV) seroprevalence of 25% (13/52) (Figure 2 and Table 2). A study carried out by Zaharaddeen Samaila et al., 2021 in Nigeria found similar results to this study in their different sample collection areas: 20%, 22%, and 31% in Zamfara, Kaduna, and Lere states respectively (Zaharaddeen Samaila et al. 2021).

The highest prevalence was found in an area closer to the river (Kolebougou site) among the other collection sites (Figure 2 and Table 2). The results in Table 3 are in

Table 2. Distribution of samples according to collection sites and serological results.

Collection site	Serology OkMV	
	Negative (%)	Positive (%)
RPI Diakitebougou	2 (3.6)	0 (0)
RPI boarding garden	0 (0)	1 (1.8)
RPI garden near bridge	1 (1.8)	1 (1.8)
RPI garden	5 (9.1)	1 (1.8)
Kolebougou	5 (9.1)	10 (18.2)
Koulikoro Downtown	5 (9.1)	0 (0)
Niarebougou	24 (43.6)	0 (0)
Total	42 (76.3)	13 (23.6)

Table 3. Classification of symptoms according to optical density.

Symptoms	Number	Optical density mean
Mosaic	0	0
Leafroll	0	0
Waffling	0	0
Mosaic + Leafroll	12	2.865
Mosaic + Leafroll + Waffling	0	0
Mosaic + Waffling	0	0
Mosaic + Leafroll + Yellow spots	1	4.023

agreement with the research work of Kouamé (2016) in Ivory Coast who mentioned that the symptom groups (mosaic plus embossing plus upward curl and embossing plus upward curl) as well as the group (mosaic plus 14.52%. Several studies report variation in the incidence of okra virus disease by symptoms and geographical areas (Kouame, 2016). Appiah et al., 2020, reported more cases of okra mosaic virus (OkMV) than okra yellow vein mosaic virus (OYVMV) in symptomatic okra leaves in their study. However, they also reported that okra yellow vein mosaic virus was more abundant than OkMV (Appiah et al. 2020). A study in Ghana reported the incidence of okra mosaic disease varying from 78 to 83% and okra leaf curl disease varying from 63 to 70% (Asare-Bediako et al., 2014b). Moreover, Asare-Bediako in 2019 reported that okra mosaic diseases are commonly observed in okra crops in Ghana, with disease incidence up to 100% depending on the okra cultivar and growth stage (Asare-Bediako 2019). According to Konaté et al. (1995), the average incidence varies by geographical area, 51% for Sahelian zone, 36% for Savannah-Sudanese zone, and 39% for north Guinean zone (Konaté et al., 1995). Osundare et al., 2024, showed that okra mosaic virus (Okmv) susceptibility, viral incidence, and disease severity are cultivar-dependent.

Successful okra mosaic disease management is very important in order to improve crop yields. Different methods can therefore be used, such as preventing the insect vector contacting the early stage plant (Fajinmi and Fajinmi, 2010), treating the plant with plant extracts (Ali et al., 2005; Asare-Bediako et al., 2014a), induced plant resistance, and chemical control of insect vectors (pesticide) (Asare-Bediako et al., 2014b; Nagendran et al., 2017). According to Fajinmi and Fajinmi (2010), in order to prevent okra mosaic virus disease (OKMV), it is necessary to control the vectors by using a 2 m high net barrier around okra plots, until the plants become more than 21 days old after emergence. Hence, an effective control measure is essential during the early stages of okra growth (Fajinmi and Fajinmi, 2010). It has also been reported in Ghana that majority of the farmers (75%) managed with synthetic pesticides (Asare-Bediako et al., 2014b).

One of the strengths of the study is the choice of a vegetable cultivation area. However, there are few limitations. Some of these are the limited number of samples tested, which makes it difficult to generalize to other okra cultivation areas in Mali, the descriptive nature of the study, and the lack of recent studies in the literature on the prevalence of OKMV. Further research is necessary to consider the severity, environmental factors (such as temperature, humidity, and soil conditions) with OKMV, and molecular characterization; however, this study provides information on the possible circulation of this virus in Mali, which constitutes a valuable addition to future research work.

Conclusion

This study shows the presence of okra mosaic virus in Mali. This is the first time OkMV has been found in Mali. However, molecular characterization is necessary to identify the viruses involved and to evaluate the incidence of okra mosaic disease at the national level, especially according to the symptoms of the geographical location.

CONFLICT OF INTERESTS

The authors have declared any conflict of interests.

ACKNOWLEDGEMENT

The authors thank Valérie Verdier of IRD - France and Professor Daouda Koné of UFHB in Abidjan – Côte d'Ivoire for their support.

REFERENCES

Ali S, Khan MA, Habib A, Rasheed S, Iftikhar Y (2005). Management of yellow vein mosaic disease of okra throughpesticide/bio-pesticide and suitable cultivars. International Journal of Agriculture and Biology 7(1):145-147.

Appiah AS, Amiteye S, Boateng F, Amoatey HM (2020). Evaluation of okra (*Abelmoschus esculentus* L. Moench) cultivars for resistance to okra mosaic virus and okra yellow vein mosaic virus. Australasian Plant Pathology 49:541-550.

Asare-Bediako E, Addo-Quaye A, Bi-Kusi A (2014a). Comparative efficacy of plant extracts in managing whitefly (B*emisia tabaci* gen) and leaf curl disease in okra (*Abelmoschus esculentus* l). American Journal of Agricultural Science and Technology 2(1):31-41. https://doi.org/doi:10.7726/ajast.2014.1004

Asare-Bediako E, Van der Puije GC, Taah KJ, Abole EA, Baidoo A (2014b). Prevalence of Okra Mosaic and Leaf Curl Diseases and Podagrica spp. Damage of Okra (*Albelmoschus esculentus*) Plants. International Journal of Current Research and Academic Review 2(6):260-271.

Asare-Bediako E, Agyarko F, Verbeek M, Taah KJ, Asare A, Agyei FK, Sarfo J, Eghan MJ, Combey R (2017). Variation in the susceptibility of okra (*Abelmoschus esculentus* L. Moench) genotypes to okra mosaic virus and Podagrica species under field conditions. Journal of Plant Breeding and Crop Science 9(6):79-89.

Asare-Bediako E (2019). Viral Diseases of Okra in Ghana and Their Management. In: Plant Pathogens. Apple Academic Press 12 p.

Fajinmi AA, Fajinmi OB (2010). Incidence of okra mosaic virus at different growth stages of okra plants (*Abelmoschus esculentus* (L.) Moench) under tropical condition. Journal of General and Molecular Virology 2(1):28-31.

Fondio L, Kouame C, Djidji AH, Traore D (2011). Caractérisation des systèmes de culture intégrant le gombo dans le maraîchage urbain et périurbain de Bouaké dans le Centre de la Côte d'Ivoire. International Journal of Biological and Chemical Sciences 5(3):1178-1189. https://doi.org/10.4314/ijbcs.v5i3.72251

Givord L (1977). Identification de souches du virus de la mosaïque du Gombo (Okra Mosaïc Virus). Annales de Phytopathologie 9(1):53-70.

Givord L, Hirth L (1973). Identification, purification and some properties of a mosaic virus of okra (*Hibiscus esculentus*). Annals of Applied Biology 74(3):359-370. https://doi.org/10.1111/j.1744-7348.1973.tb07756.x

Haruna IM, Jabil IY (2017). Survey on the effect of okra mosaic virus and leaf curl virus on yield in Maiduguri, Borno State, Nigeria. International Journal of Science and Applied Research 2(3):1-7.

Kadri A, Moussa OZ, Yacouba AS, Abdou KH, Karimoune L (2013). Gestion intégrée de Maruca vitrata (FABRICIUS, 1787) et Megalurothrips sjostedti (TRYBOM, 1908), deux insectes ravageurs majeurs du niébé au Niger. International Journal of Biological and Chemical Sciences 7(6):2549-2557. https://doi.org/10.4314/ijbcs.v7i6.29

Khomsug P, Thongjaroenbuangam W, Pakdeenarong N, Suttajit M, Chantiratikul P (2010). Antioxidative activities and phenolic content of extracts from okra (*Abelmoschus esculentus* L.). Research Journal of Biological Sciences 5(4):310-313.

Konaté G, Barro N, Fargette D, Swanson MM, Harrison BD (1995). Occurrence of whitefly-transmitted geminiviruses in crops in Burkina Faso, and their serological detection and differentiation. Annals of Applied Biology 126(1):121-129. https://doi.org/10.1111/j.1744-7348.1995.tb05008.x

Kouame AC (2016). Symptomatologie des maladies virales du gombo (Abelmoschus esculentus) et leur impact potentiel sur le rendement. Mémoire de Master, UFR des Sciences de la nature. Université Nangui Abrogoua, Côte d'Ivoire P 50.

Kumar S, Dagnoko S, Haougui A, Ratnadass A, Pasternak D, Kouamé C (2010). Okra (*Abelmoschus* spp.) in West and Central Africa: Potential and progress on its improvement. African Journal of Agricultural Research 5(25):3590-3598.

Nagendran K, Pandey KK, Rai AB, Singh B (2017). Viruses of Vegetable Crops: Symptomatology, Diagnostics and Management. IIVR Technical Bulletin No. 75, IIVR, Varanasi P 48

N'Guessan KP, Fargette D, Fauquet C, Thouvenel J (1992). Aspects off the epidemiology of okra leaf curl virus in Côte d'Ivoire. Tropical Pest Management 38(2):122-126. https://doi.org/10.1080/09670879209371668

Osundare O, Oyebamiji KJ, Okonji CJ, Fayemiro OS, Fajinmi AA (2024). Incidence and Severity of Okra Mosaic Virus on Field-grown Three Cultivars of Okra (*Abelmoschus Esculentus* L.). Jordan Journal of Agricultural Sciences 20(1):41-47.

Ouoba KH, Desmorieux H, Zougmore F (2010). Caractérisation du séchage convectif du gombo, influence de la découpe et de ses constituants. Afrique Science 6(2):37-48.

Tiendrébéogo F, Traoré VSE, Lett J-M, Barro N, Konaté G, Traoré AS, Traoré O (2010). Impact of okra leaf curl disease on morphology and yield of okra. Crop Protection 29(7):712-716. https://doi.org/10.1016/j.cropro.2010.02.007

Ugwoke KI, Onyishi LE (2009). Effects of Mycorrhizae (*Glomus musae*), Poultry Manure and Okra Mosaic Potyvirus (Okmv) on Yield of Okra (*Abomoscus esculentus*). Production Agriculture and technology 5(2):359-369.

Zaharaddeen Samaila G, Boniface DK, Banwo OO, Dada AM, Agart CC, Tijjani I (2021). Occurrence and Distribution of Viruses Associated with Okra and Their Alternative Hosts in Kaduna and Zamfara States, Nigeria. Journal of Tropical Crop Science 8(3):177-186. https://doi.org/10.29244/jtcs.8.03.177-186.

Vol. 23(4), pp.152-161, April 2024
DOI: 10.5897/AJB2024.17657
Article Number: CED1E7A72105
ISSN: 1684-5315

http://www.academicjournals.org/AJB

ACADEMIC JOURNALS
expand your knowledge

African Journal of Biotechnology

Full Length Research Paper

Evaluation of runs of homozygosity and genomic endogamy in the Creole breeds Guaymi and Guabala in Panama

Axel Villalobos-Cortés[1]*, Ginnette Rodríguez-Espino[2] and Selma Franco-Schafer[3]

[1]Animal Conservation and Improvement, Laboratory of Analysis and Applied Molecular Biology (LABMA), City of Knowledge, IDIAP, Panama.
[2]Animal production IDIAP, El Ejido Experimental Station, Panama.
[3]Veterinary Epidemiology, Animal Health Laboratory, IDIAP, Divisa, Panamá.

Received 11 February, 2024; Accepted 8 April, 2024

The inbreeding coefficient measures the likelihood of identical alleles at a locus in a population due to descent from a common ancestor, highlighting potential negative impacts on health and fitness in both natural and domesticated populations. This study focuses on homozygous segments continuous genomic regions of homozygosity resulting from the inheritance of identical haplotypes from both parents and their role in assessing genomic inbreeding and understanding genetic history and relationships within populations. Such analysis can reveal recessive disease risks. Specifically, the research assessed homozygous segments and the genomic inbreeding coefficient in Creole cattle breeds Guaymi and Guabala in Panama using 10,000 single nucleotide polymorphisms (SNP) markers. Findings showed significant differences in homozygosity between breeds, with Guabala exhibiting higher inbreeding levels, suggesting varied breeding histories or intense selection. The study also detected homozygosity patterns indicating genetic links or shared ancestors between breeds, underscoring the impact of environmental factors and human intervention on genetic diversity. Geographic isolation and artificial selection were key influences on the genetic structures of Guaymi and Guabala breeds, respectively. This underscores the balance between maintaining genetic diversity for adaptability and selecting for desirable traits, emphasizing the importance of managing genetic health and biodiversity for sustainable population viability.

Key words: Bioinformatics, biotechnology, genomics, creole, livestock, conservancy, Guaymi, Guabala, Panama.

INTRODUCTION

The inbreeding coefficient (F) is defined as the probability that two alleles at a randomly sampled locus in a population are identical by descent (IBD) relative to a base population in which all alleles are independent (Wright, 1922). Inbreeding is the result of mating between closely related individuals, and the resulting detrimental

*Corresponding author. E-mail: villalobos.axel@gmail.com.

effects on progeny performance and fitness have been widely documented in both natural and domesticated animal populations (Bjelland et al., 2013).

Runs of homozygosity (ROH) are contiguous regions of the genome in which an individual is homozygous at all sites (Gibson et al., 2006). ROHs arise when two copies of an ancestral haplotype come together in an individual. Consequently, this haplotype is autozygous, that is, homozygous by descent (Ceballos et al., 2018).

ROH in cattle have been used to analyze the history of a population after a recent selection event (Purfield et al., 2012), to estimate the coefficients of consanguinity (Ferencakovic et al., 2011, 2013), to study the detrimental effects of inbreeding on the characteristics that affect the profitability of a farm (Bjelland et al., 2013) and to control the increase in inbreeding in cross designs assisted by genome analysis (Pryce et al., 2012).

A fundamental aspect in the study of genomic homozygosity is islands of ROH. Unlike homozygous segments, which include any genomic area where the alleles of homologous chromosomes are identical, a situation that can arise both by inbreeding and randomly, especially in short regions of the genome (Purfield et al., 2012), ROH islands specifically refer to homozygous segments that are remarkably extensive and/or frequent in a population. These islands are of special relevance in population genetics since they can indicate histories of inbreeding or natural selection processes or even be linked to certain diseases or phenotypic characteristics (Toro-Ospina et al., 2022).

The study of genomic inbreeding based on ROH can provide important information about the genetic history and kinship relationships within a population. It may also have health implications, as homozygous regions may contain rare genetic variants associated with recessive diseases. Furthermore, genomic inbreeding can affect the viability and general health of a population through the loss of genetic diversity and the appearance of deleterious recessive traits (Ferencakovic et al., 2013; Forutan et al., 2018).

The coefficient of inbreeding F_{ROH} is a specific parameter that is related to ROH and is used to quantify genomic inbreeding based on ROH in an individual or a population (Scienscki et al., 2019). The F_{ROH} coefficient is calculated by dividing the sum of the lengths of all the ROH segments in an individual's genome by the total length of the autosomal genome (Peripolli et al., 2018a).

Principal Component Analysis (PCA) is a widely used statistical technique in population genetics to identify structures in the distribution of genetic variation across geographical locations and ethnic origins. It has been applied in livestock to analyze single nucleotide polymorphisms (SNPs) data to detect population structures and potential outliers, as well as to identify small panels of genetic markers that can be used to trace the origin of unknown livestock samples. For instance, Abraham and Inouye (2014) developed flashpca, a highly efficient PCA implementation based on randomized algorithms, capable of performing PCA on large SNP datasets much faster than existing tools, without losing accuracy in extracting the principal components (Abraham and Inouye, 2014).

Creole cattle are significant genetic assets because of their exceptional adaptation to local environments and their resistance to diseases. A thorough genetic characterization, encompassing Runs of Homozygosity (ROH) analysis, islands of ROH, and F_{ROH}, can provide valuable insights for the conservation of these breeds (Gaspar et al., 2023). This process is instrumental in identifying unique genetic markers and devising strategies for the sustainable preservation and utilization of these valuable genetic resources. Conversely, inbreeding poses a risk by potentially increasing the prevalence of harmful alleles, which can diminish individual fitness and the overall viability of the population (Dixit et al., 2020). By quantifying F_{ROH}, we can gauge the levels of inbreeding and assess its possible effects on the health, productivity, and genetic robustness of these breeds. This evaluation is especially vital for conservation and breeding programs aimed at sustaining healthy populations while safeguarding their distinctive genetic characteristics (Liu et al., 2022). The objective of this work was to evaluate the ROH and quantify the genomic inbreeding coefficient derived from the ROH (F_{ROH}) of the Creole cattle breeds Guaymi and Guabala in Panama.

MATERIALS AND METHODS

Thirty-four samples from the Creole cattle breeds Guabala (15) and Guaymi (19) selected from an array of 10,000 SNP markers were analyzed using a DNA sequencer from the company Affymetrix as part of the Innovative Management of Animal Genetic Resources (IMAGE) project sponsored by the FAO. The objective of this project is to develop and provide free, publicly accessible multi-species single nucleotide polymorphism (SNP) arrays tailored for major farm animal species. These arrays are designed to genotype genetic collections at an affordable cost, aiming to keep expenses under $20 per sample https://www.imageh2020.eu/conteudo.php?idm=18&lang=en. Five milliliters of venous blood were taken from the jugular area of each animal. The samples were collected in tubes with EDTA and kept in a container with ice until their arrival at the laboratory, where they were immediately processed. DNA extraction was carried out using a commercial DNeasy Blood and Tissue Kit from Qiagen (Germany), for which the average concentration was 45 ng/ml and the volume was 50 µL per sample, for a total amount of 2.5 µg of DNA. The extracted DNA was sent to the company Affymetrix in the Netherlands for analysis. This work complied with the Nagoya Protocol for Access and Benefit Sharing of Genetic Resources (FAO, 2019) through a material transfer agreement (MTA) between the Institute of Agricultural Innovation and Wagenigen University and transfer permit # SEX/A-1-2021 from the Ministry of the Environment of the Republic of Panama.

Of the 10,000 SNPs selected, 8,416 met the company's quality control criteria. All the SNPs were aligned with the reference genome (*Bos taurus* UMD 3.1.1/bos Tau8). Once the data were obtained, quality control was carried out to eliminate the SNPs that did not meet the established criteria (filtered SNPs with a high failure rate, SNPs with high variability and SNPs in linkage

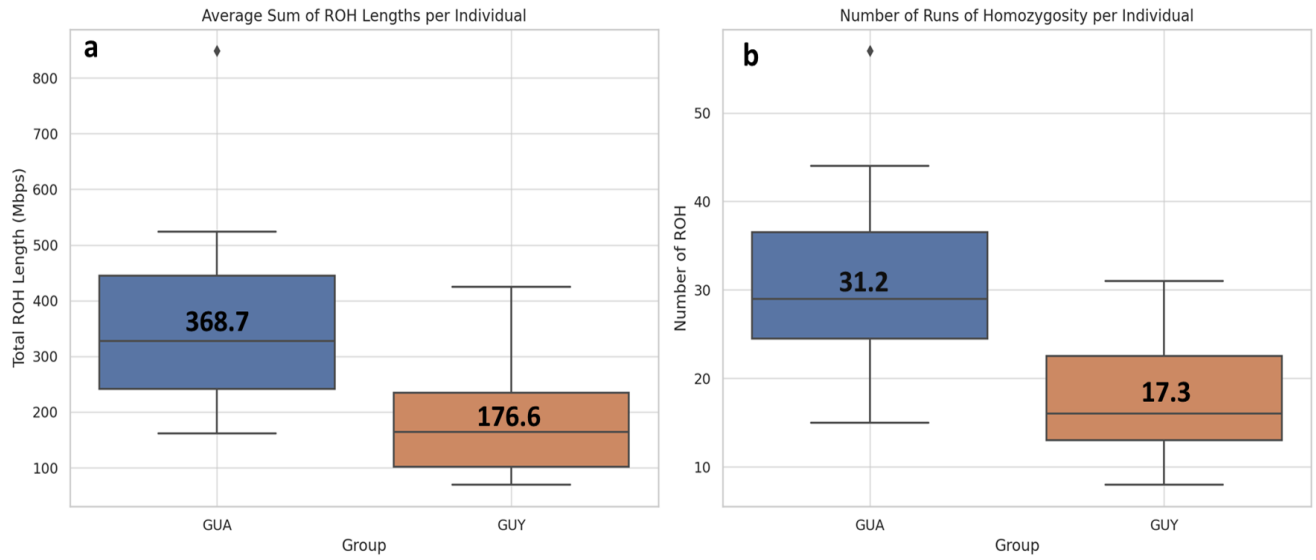

Figure 1. (a) Average length of ROH by population; (b) average number of ROH per population.

disequilibrium) using the PLINK 1.9 program in the R and RStudio platforms. The following criteria were applied: loss by SNP, --gene (0.1), losses per individual, --mind (0.1), minor allele frequency, --maf (0.05), and deviations from Hardy equilibrium -Weinberg --hwe (0.001). After quality control, there remained 7,282 SNP variants that fulfilled the quality control criteria.

The ROH were estimated for each individual separately and subsequently classified into five categories according to length (0-2, 2-4, 4-8, 8-16, and > 16 Mb) following the classification methods used in similar studies (Kirin et al., 2010; Marras et al., 2015). For each ROH category in both breeds, the total number of ROH per breed (nROH), percentage of ROH per breed (%ROH), and mean number of ROH per breed (M_{ROH}) were calculated.

To identify islands of homozygosity, a comparative analysis of ROH between individuals was performed. The runs were grouped by their genomic location, considering as islands those regions of homozygosity that appeared in a significant percentage of the population. An initial threshold of 50 to 20% was established until the presence of at least one island of ROH was determined. ROH that overlapped or were close to each other in at least 20 to 50% of the individuals were considered part of an island of ROH.

To carry out the genomic inbreeding analysis, two parameters were used. First, the F_{ROH} coefficient was calculated by determining the ratio of the length of the genome found in ROH to the total length of the genome covered by the SNPs using PLINK 1.9 software (Purcell et al., 2007). The second parameter was the inbreeding coefficient, focusing especially on the F_{HOM} coefficient, which is based on the difference between the observed and expected number of homozygous genotypes; this analysis was also performed using PLINK 1.9 (Purcell et al., 2007). To complement the genetic study of the Guaymi and Guabala cattle populations, a Principal Component Analysis (PCA) was carried out using the PLINK 1.9 software (Purcell et al., 2007), utilizing the dataset of 7,200 SNP data that passed quality control. The analysis allowed for summarizing the genetic variation in a few dimensions representing the largest sources of variability among the samples. The PCA provides an additional perspective on the genetic structure of the studied populations, complementing the ROH and genomic inbreeding analyses for a better understanding of diversity and inbreeding in these Creole breeds.

RESULTS AND DISCUSSION

One of the critical considerations of this study is the sample size analyzed. The populations of the Guaymi and Guabala breeds examined come exclusively from conservation centers, where their genotype is known, and their genetic purity is guaranteed. This methodological selection was intentionally designed to ensure that the analyses accurately reflect the inherent genetic structure of these breeds, free from external genetic contamination that could distort interpretations of inbreeding and genetic diversity. However, it is important to acknowledge that, although this strategy ensures the authenticity of the samples, it also limits the generalization of our findings to all populations of these breeds. The representativeness of our samples is affected by the fact that, even within conservation centers, the populations of Guaymi and Guabala are relatively small. This implies that any extrapolation of our results to the general populations of these breeds must be done with caution.

The evaluation of the ROH in the Guabala and Guaymi cattle populations revealed notable differences. In the Guabala cattle, 14 ROH were identified, with an average length of approximately 1468.45 kb. On the other hand, in the Guaymi cattle, 11 ROH were found, with an average length of 1004.48 kb. These findings suggest a greater extent and number of ROH in Guabala cattle, indicating differentiated levels of inbreeding or different breeding histories between the two populations.

Similarly, Figure 1a shows that the total length of the ROH in the Guabala cattle, with 368.70 Mega base pairs (Mbps), was greater than that reported in other breeds, such as Hereford, with 378 Mbps (Szmatola et al., 2019), and significantly greater than that in *Bos indicus* breeds,

Table 1. Descriptive statistics of homozygous individuals, total number of ROHs by race (nROH), percentage of ROHs by race (% ROH) and mean number of ROHs by race (M ROH).

Categories (Mb)	nROH		% ROH		M_{ROH}	
	GUA	GUY	GUA	GUY	GUA	GUY
0-2	26	32	5.60	9.70	0.71	1.18
2-4	26	22	5.60	6.70	2.72	2.96
4-8	123	90	26.30	27.40	6.18	6.42
8-16	193	135	41.20	41.00	11.17	11.02
> 16	100	50	21.40	15.20	25.26	23.76

such as Gyr, 211 Mbps; Haryana, 106 Mbps; Ongole, 188 Mbps; and Kangayan, 283 Mbps (Dixit et al., 2020). The Guaymi breed, with an average of 176.65 Mbps, had a shorter total length of ROH, similar to that observed in the Blanco-Orejinegro breed (170.36 Mbps) (Caivio-Nasner et al., 2021).

Regarding the average number of ROHs per individual, that in the Guabala cattle was 31.20, while that in the Guaymi cattle was 7.32. This difference suggested variability in genetic structure between the two groups, with the Guabala cattle exhibiting more homozygous events. These values are lower than those of the Hereford breed (80.6 ROH per individual) and higher than those of several native Polish breeds (such as White-Backed (23.9), Polish Red (23.3), and Polish Red-and-White (21.8)); lower than those of Indica breeds, such as Kangayan (63.6), Gyr (45.3), and Ongole (44.9); higher than those of the Tharpakar (24.6), Hariana (26.3), and Sahiwal (24.6) breeds; and higher than White Orejinegro breed, which has a low value of 18.35 (Szmatola et al., 2019; Dixit et al., 2020; Caivio-Nasner et al., 2021).

The five length categories of the ROH (homozygous segments): 0-2, 2-4, 4-8, 8-16, and > 16 Mb (Table 1). In the short-length categories (0-2 and 2-4 Mb), both breeds exhibited similar numbers of ROH, suggesting comparable homozygous patterns. On the other hand, in the intermediate and long length categories, the Guabala breed had a greater number of ROH, which may be indicative of greater consanguinity in these segments. These findings are consistent with previous studies on inbreeding and genetic diversity in these populations (Purfield et al., 2012; Scienski et al., 2021).

Regarding the percentage of the genome covered by ROH (%ROH), the short segments of both populations suggest that there is still a level of genetic diversity, although the reported values are contrary to those observed in Holstein cattle in China by Liu et al. (2021), who reported higher percentages of these short genome segments. Comparable results were reported by Peripolli et al. (2018a) in Nellore cattle from Brazil. Short ROH are often associated with older shared ancestry and less immediate inbreeding (Sumreddee et al., 2020). On the other hand, the high percentage of ROH in the medium and long segments in both populations indicates a significant level of inbreeding (Peripolli et al., 2018b). This information is consistent with the way in which the Guabala breed developed within the Castrellón family, who described the formation of this breed as being driven by the selection of the color red among other traits.

The analysis of the mean number of ROH by breed (M_{ROH}) revealed notable differences between the Guaymi and Guabala breeds. The Guaymi breed originated in the mountainous areas of the Gnobe-Buglé region, such as Tolé and Cerro Plata, and the Guabala breed was developed by the Castrellón family in the Guabala area through selection for color and other characteristics of interest (Villalobos et al., 2010). The data revealed intriguing patterns of homozygosity in both populations. In the shorter segments (0-2 and 2-4 Mb), the Guaymi population consistently presented higher mean numbers of ROH than did the Guabala. This finding suggested greater homozygosity, which could be indicative of a smaller effective population size or a lower genetic flow with other populations, possibly due to the geographic isolation inherent to its location and later confinement to conservation centers (Addo et al., 2021). These factors could have contributed to greater fixation of homozygous alleles in the short and middle segments of the genome. On the other hand, in the longest segments (especially> 16 Mb), an inverse pattern was observed with the Guabala breed showing a greater mean number of ROH. This observation is consistent with the effects of artificial selection practiced by the Castrejon family that developed this breed in lowland areas in the eastern region of the Chiriquí province (Villalobos et al., 2010). Selection directed toward specific characteristics, such as color, could have led to the fixation of certain alleles, resulting in long stretches of homozygous DNA. This pattern is indicative of an intensive selection process, which in turn reduces genetic diversity in specific regions of the genome (Liu et al., 2022).

These results highlight how environmental factors and human action can significantly influence the genetic makeup of populations (Beishova et al., 2022). In the Guaymi breed (originated in the mountainous regions of the Ngäbe-Buglé comarca), natural factors such as geographic isolation seem to play a crucial role in the development of homozygosity, while the genetic makeup of the Guabala breed has been shaped by human interventions through artificial selection. These findings

Figure 2. Genomic inbreeding coefficient of the Guaymi and Guabala breeds

provide a deeper understanding of how selection practices and environmental factors can direct the genetic evolution of populations.

In the study of population genetics, the identification of ROH is crucial for understanding genetic diversity and evolutionary history. After adjusting the threshold to 20%, significant islands of ROH were identified in the populations studied, standing out on three specific chromosomes:

1. Chromosome 15: A segment from 51,528,617 to 59,333,016 common to approximately 20.59% of individuals.
2. Chromosome 16: A segment from 25,623,468 to 26,455,382, shared by approximately 35.29% of individuals.
3. Chromosome 18: A segment between 63,878,550 and 65,978,584, shared by approximately 23.53% of individuals.

These ROH segments are shared by individuals of the Guabala and Guaymi breeds, which suggest a history of genetic exchange between these groups or a common ancestor. This observation indicates shared genetic diversity, possibly reflecting past evolutionary or migratory events (Gaspar et al., 2023; Mulim et al., 2022). The presence of these genes with important functions in both groups could indicate natural selection in a shared environment (Szmatoła et al., 2019).

The intraracial homogeneity in the Guabala breed, evidenced by the shared segments with ROH, could be derived from historical selection practices in animals. For example, the Castrellón family has maintained certain characteristics, such as red coloration and traits of Spanish origin, while avoiding crosses with *Bos indicus* breeds (Villalobos et al., 2010; Martinez et al., 2012). This trend is not unusual in populations with histories of relative isolation and may be a result of inbreeding and inheritance of identical alleles from common ancestors (Gorssen et al., 2021).

The uniqueness of the Guabala breed reflects a specific subpopulation characterized by marked genetic homogeneity. In the context of significant artificial selection, such homogeneity is expected and often intentional, with ROH acting as markers of this genetic uniformity (Scienski et al., 2019).

Considering the evolutionary implications, natural selection and consequences for the health and biodiversity of these populations is essential. The presence of ROH suggests that certain genetic characteristics were favored throughout the evolution of the group in response to specific environmental pressures (Goszczynski et al., 2018). However, genetic homogeneity, although beneficial for the perpetuation of desirable traits, can limit the ability of a population to adapt to new environmental or health challenges, affecting its long-term viability (Medugorac et al., 2011).

The F_{ROH} coefficient is a quantitative measure of autozygosity that reflects the proportion of the genome that consists of segments of homozygosity by descent. The Guabala population had an average F_{ROH} of 0.147 ± 0.066, which is indicative of greater inbreeding than the Guaymi population, for which the average F_{ROH} was 0.071 ± 0.035.

The violin plot (Figure 2) shows not only the medians and quartiles but also the density of the distribution of the

Table 2. Values of F_{ROH} at the chromosome level (Chr) in the races Guabala (GUA) and Guaymi (GUY).

Chr	GUA	GUY
Chr1	0.199	0.129
Chr2	0.150	0.146
Chr3	0.270	0.126
Chr4	0.159	0.098
Chr5	0.187	0.111
Chr6	0.200	0.106
Chr7	0.237	0.114
Chr8	0.271	0.261
Chr9	0.280	0.151
Chr10	0.274	0.155
Chr11	0.165	0.162
Chr12	0.220	0.235
Chr13	0.161	0.151
Chr14	0.165	0.180
Chr15	0.158	0.180
Chr16	0.171	0.184
Chr17	0.430	0.179
Chr18	0.145	0.093
Chr19	0.195	0.168
Chr20	0.110	0.076
Chr21	0.145	0.107
Chr22	0.183	0.315
Chr23	0.245	0.115
Chr24	0.350	0.309
Chr25	0.256	0.377
Chr26	0.268	0.225
Chr27	0.270	0.310
Chr28	0.403	0.206
Chr29	0.292	0.182

F_{ROH} values, offering a comprehensive visualization of the intrapopulation genetic variability (Wu et al., 2021). The wide dispersion observed in the Guabala population suggests more pronounced variability in consanguinity, possibly due to mating practices between related individuals or a more subdivided population structure. In contrast, the narrower distribution in the Guaymi population points to less consanguinity and, by inference, greater genetic heterogeneity. The F_{ROH} values observed for the Guabala breed are greater than those reported by Zinovieva et al. (2020) for the native breeds of Russia, Yaroslavl (0.103) and Kholmogor (0.059). La Guaymi had an intermediate range. Determination of the coefficient of inbreeding based on ROH has several advantages compared to the classical coefficient of inbreeding calculated on the basis of pedigree data (Szmatoła et al., 2019; Toro-Ospina et al., 2022). F_{ROH} more efficiently predicts the degree of genome autozygosity and can be estimated in any animal with genotypic data, even if genealogical information is unavailable (Ferencakovic et al., 2011; Purfield et al., 2012; Curik et al., 2014). Importantly, all regions of homozygosity have an impact on phenotypes, which suggests that genetic conservation strategies could focus on maintaining diversity in critical chromosomal regions (Peripolli et al., 2017).

This may be particularly relevant for small or isolated populations in which genetic diversity is limited and inbreeding can have more pronounced effects, such as the Guabala and Guaymi breeds (Pilon et al., 2021).

The differences between the Guabala and Guaymi breeds were evidenced by the techniques described above. Furthermore, these differences are manifested in a more complex way, not only in terms of population inbreeding levels but also at the chromosomal level, shown in Table 2.

A detailed analysis of the genomic inbreeding coefficient by chromosome in the Creole cattle breeds Guabala and Guaymi, revealed notable differences. In the Guabala breed, the chromosome that stands out the most due to its high level of inbreeding is 17, with a F_{ROH}

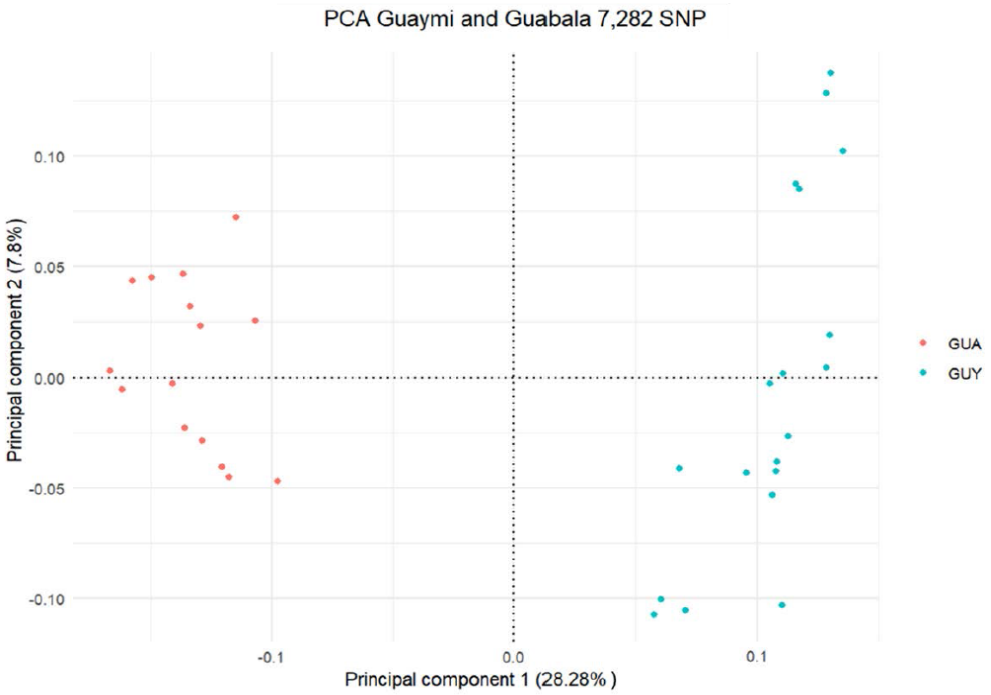

Figure 3. Principal components analysis of Guaymi and Guabala breeds.

of 0.430, indicating a significant level of inbreeding. On the other hand, chromosome chr20 showed the lowest level of inbreeding in this breed, with a F_{ROH} of only 0.109.

In the Guaymi breed, chromosome 25 was the most affected by inbreeding, with a F_{ROH} of 0.377, also indicating a high level of inbreeding. Like in the Guabala breed, chromosome 20 in the Guaymi breed showed the lowest level of inbreeding (0.076). This parallelism on chromosome 20 between the two breeds is remarkable, suggesting that this chromosome could be less susceptible to inbreeding in these bovine breeds.

The variability in the F_{ROH} values between the chromosomes of the Guabala and Guaymi breeds can have significant biological implications, particularly in the context of genetic selection and diversity (Toro-Ospina et al., 2022). These results are indicative of the degree of homozygosity in the genome. Greater homozygosity, reflected in high values, could indicate a reduction in genetic diversity, which in turn may be the result of inbreeding or a small founder population (Kim et al., 2019).

Variations in genomic inbreeding between different chromosomes can indicate differences in genetic diversity throughout the genome, which could impact the adaptive capacity of the population to environmental changes or diseases (Hohenlohe et al., 2021; Beishova et al., 2022).

Specific differences in F_{ROH} values between chromosomes could suggest the presence of selection signatures (de Simoni et al., 2014; Gorssen et al., 2021). For example, if certain chromosomes in a breed consistently show higher homozygosity, this could be indicative of selection, either natural or artificial, for specific genetic traits. Among the chromosomes on which the Guaymi breed shows superiority to the Guabala breed, it is possible that there are genes or chromosomal regions that have been the object of selection, leading to greater homozygosity in these specific areas (Saravanan et al., 2021). High homozygosity may be associated with an increased risk of genetic diseases, particularly those involving harmful recessive genes. Understanding the distribution of homozygosity along chromosomes is crucial for the management of breeding and conservation of these breeds, allowing the development of strategies to minimize the health risks associated with inbreeding (Kardos et al., 2016).

The differences between the Guaymi and Guabala breeds, and specifically between chromosomes, could reflect their evolutionary and demographic histories, including events such as genetic bottlenecks, population expansions or migrations, which have been discussed in this work and by other authors (Murray et al., 2010; da Fonseca et al., 2019).

In the present study, the genetic structure and diversity of the Guaymi and Guabala Creole breeds are examined through PCA (Figure 3). This technique has allowed a detailed visual evaluation of the genetic differentiation existing between both populations. The results obtained from the PCA highlight that the first principal component

(PC1) is responsible for 28.28% of the total observed variability, demonstrating a notable genetic distinction between the studied breeds. This degree of genetic differentiation suggests that both selective practices and environmental factors have contributed to a significant genetic divergence between the breeds, possibly reflecting adaptations to specific ecological niches or a history of selection oriented towards various phenotypic traits. On the other hand, the second principal component (PC2), which explains 7.8% of the variability, reveals the internal diversity within each breed, pointing to an underlying genetic heterogeneity. This internal variability could indicate the presence of subpopulations within the breeds or differences in inbreeding and gene flow. For example, the variability observed in the Guaymi breed may suggest a lower susceptibility to inbreeding, attributable to its origin in isolated mountainous regions. In contrast, the genetic structure of Guabala could reflect a history of more intense selection for certain phenotypic traits, such as coat color, influenced by human intervention. The assessment of the genetic structure and diversity of cattle breeds through advanced genomic analyses, such as Principal Component Analysis (PCA) and the identification of runs of homozygosity (ROH), has proven to be an essential tool for understanding genetic differentiation and the adaptation of breeds to specific ecological niches or to varied selection pressures. As observed in the study by Toro-Ospina et al. (2022), where the Criollo Caqueteño cattle breed in Colombia was analyzed, the application of these genomic methods allowed for the detection of a decrease in inbreeding frequency and the identification of genomic regions associated with economically interesting traits. This methodological approach reflects a remarkable genetic distinction and internal diversity within the studied breeds, like what is observed in our analysis of the Creole Guaymi and Guabala breeds through PCA, highlighting the importance of selective practices and environmental factors in the genetic divergence between breeds (Toro-Ospina et al., 2022). Similar to our analysis of the Creole Guaymi and Guabala breeds using Principal Component Analysis (PCA), the study by Barbato et al. (2020) provides a valuable perspective on the genetic structure and diversity in cattle populations, highlighting the importance of ancestral selection and environmental factors in the genetic differentiation among populations.

The configuration of the points in the PCA plot, and particularly the clustering of individuals from the Guabala breed, supports the hypothesis of a higher degree of inbreeding in this population, as discussed earlier. Moreover, the dispersion observed in the Guaymi breed could indicate a reduced incidence of inbreeding or a greater residual genetic diversity. These findings are of vital importance for conservation strategies and management of these breeds, providing a framework for future research on their genetic conservation.

To advance the study of the Guaymi and Guabala Creole bovine breeds, three key areas of focus are suggested. First, it is essential to conduct genomic wide association studies (GWAS) to discover genetic variants linked to desirable traits and recessive diseases. This information is necessary for the design of effective breeding programs and the conservation of these breeds. Second, given the observed inbreeding, a comprehensive analysis of the associated health risks must be performed. Identifying recessive diseases and adverse traits will help develop breeding management strategies that minimize inbreeding and maintain genetic diversity. Finally, comparing these homozygous patterns and inbreeding coefficients with those of other bovine breeds globally will provide a broader context, revealing unique evolutionary patterns and guiding conservation strategies. These steps are critical for understanding and preserving the genetic diversity and long-term health of these breeds. In this study, the lack of access to complete historical records has limited our ability to interpret some of the genetic patterns observed in the context of historical breeding practices and population dynamics. However, the recent formation of a breeders' association, along with the enactment of a law focused on promoting the conservation and study of these Creole breeds, represents a promising step towards the collection and systematization of such historical data. This initiative will not only facilitate the preservation of crucial information for future genetic analyses but also underscores the growing recognition of the importance of integrating historical and genetic knowledge for the management and conservation of Creole breeds.

Conclusions

The present study provides a deep understanding of the genetic structure and levels of consanguinity of the Guaymi and Guabala Creole bovine breeds. The results revealed significant differences in the homozygous segments and genomic inbreeding coefficients between the two breeds. A greater extension and number of ROH segments were observed in the Guabala breed than in the Guaymi breed, which indicates different levels of inbreeding or different breeding histories. Furthermore, the identification of significant islands of ROH suggests a history of genetic exchange or a common ancestor between these groups. These findings are critical for understanding the genetic diversity and evolution of these breeds and their potential health risks associated with inbreeding. The identification of selection signatures and runs of homozygosity highlights specific areas for future research, with the potential to unlock key genetic variants for desirable traits and disease resistance. Likewise, this study serves as a call to action for strengthening collaborations between academic institutions, breeder communities, and governmental bodies, thus ensuring the long-term viability and sustainability of these valuable

bovine breeds within Panama's agro-biodiversity heritage.

CONFLICT OF INTERESTS

The authors have not declared any conflict of interests.

ACKNOWLEDGEMENTS

The authors thank Wagenigen University for support in the reception and analysis of the DNA samples, Dr. Richard Crooijmans for his collaboration in the reception of the samples, the Institute of Agricultural Innovation of Panama (IDIAP), the National Secretariat of Science, Technology and Innovation (SENACYT), and the National Research System (SNI) for their support in this research. This work was financed in part by funds from the European Union's Horizon 2020 Research and Innovation Program under grant agreement No. 677353 and in part with funds from the SENACYT National Research System.

REFERENCES

Abraham G, Inouye M (2014). Fast principal component analysis of large-scale genome-wide data. PloS One 9(4):e93766.

Addo S, Klingel S, Thaller G, Hinrichs D (2021). Genetic diversity and the application of runs of homozygosity-based methods for inbreeding estimation in German White-headed Mutton sheep. PloS One 16(5):e0250608.

Barbato M, Reichel MP, Passamonti M, Low WY, Colli L, Tearle R, Williams JL, Marsan PA (2020). A genetically unique Chinese cattle population shows evidence of common ancestry with wild species when analysed with a reduced ascertainment bias SNP panel. PLoS ONE 15(4):e0231162.

Beishova I, Dossybayev K, Shamshidin A, Belaya A, Bissembayev A, Khamzin K, Kovalchuk A, Nametov A (2022). Distribution of homozygosity regions in the genome of Kazakh cattle breeds. Diversity 14(4):279.

Bjelland DW, Weigel KA, Vukasinovic N, Nkrumah JD (2013). Evaluation of inbreeding depression in Holstein cattle using whole-genome SNP markers and alternative measures of genomic inbreeding. Journal of Dairy Science 96(7):4697-4706.

Caivio-Nasner S, López-Herrera A, González-Herrera LG, Rincón JC (2021). Diversity analysis, runs of homozygosity and genomic inbreeding reveal recent selection in Blanco Orejinegro cattle. Journal of Animal Breeding and Genetics 138(5):613-27.

Ceballos FC, Hazelhurst S, Ramsay M (2018). Assessing runs of Homozygosity: a comparison of SNP Array and whole genome sequence low coverage data. BMC Genomics 19:1-12.

Curik I, Ferenčaković M, Sölkner J (2014). Inbreeding and runs of homozygosity: A possible solution to an old problem. Livestock Science 166(1):26-34.

da Fonseca RR, Ureña I, Afonso S, Pires AE, Jørsboe E, Chikhi L, Ginja C (2019). Consequences of breed formation on patterns of genomic diversity and differentiation: the case of highly diverse peripheral Iberian cattle. BMC Genomics 20:1-13.

de Simoni Gouveia JJ, da Silva MV, Paiv SR, de Oliveira SM (2014). Identification of selection signatures in livestock species. Genetics and Molecular Biology 37(2):330-342.

Dixit SP, Singh S, Ganguly I, Bhatia AK, Sharma A, Kumar NA, Dang AK Jayakumar S (2020) Genome-wide runs of homozygosity revealed selection signatures in Bos indicus. Frontiers in Genetics 11:92.

FAO (2019). ABS Elements: Elements to facilitate domestic implementation of access and benefit-sharing for different subsectors of genetic resources for food and agriculture – with explanatory notes. FAO, Rome. 84 pp Licence: CC BY-NC-SA 3.0 IGO. http://www.fao.org/3/ca5088en/ca5088en.pdf

Ferencakovic M, Hamzic E, Gredler B, Curik I, Solkner J (2011). Runs of homozygosity reveal genome-wide autozygosity in the Austrian Fleckvieh cattle. Agriculturae Conspectus Scientificus 76(4):325-329.

Ferencakovic M, Hamzic E, Gredler B, Solberg TR, Klemetsdal G, Curik I. Solkner J (2013) Estimates of autozygosity derived from runs of homozygosity: empirical evidence from selected cattle populations. Journal of Animal Breeding and Genetics 130(4):286-293.

Forutan M, Ansari Mahyari S, Baes C, Melzer N, Schenkel FS, Sargolzaei M (2018). Inbreeding and runs of homozygosity before and after genomic selection in North American Holstein cattle. BMC Genomics 19:1-12.

Gaspar D, Usié A, Leão C, Guimarães S, Pires AE, Matos C, Ramos AM, Ginja C (2023). Genome-wide assessment of the population structure and genetic diversity of four Portuguese native sheep breeds. Frontiers in Genetics 14:1109490.

Gibson J, Newton EM, Collins A (2006). Extended tracts of homozygosity in outbred human populations. Human Molecular Genetics 15(5):789-795.

Gorssen W, Meyermans R, Janssens S, Buys N (2021). A publicly available repository of ROH islands reveals signatures of selection in different livestock and pet species. Genetics Selection Evolution 53:1-10.

Goszczynski D, Molina A, Terán E, Morales-Durand H, Ross P, Cheng H, Giovambattista G, Demyda-Peyrás S (2018). Runs of homozygosity in a selected cattle population with extremely inbred bulls: Descriptive and functional analyses revealed highly variable patterns. PLoS ONE 13(7): e0200069.

Hohenlohe PA, Funk WC, Rajora OP (2021). Population genomics for wildlife conservation and management. Molecular Ecology 30(1):62-82.

Kardos M, Taylor HR, Ellegren H, Luikart G, Allendorf FW (2016). Genomics advances the study of inbreeding depression in the wild. Evolutionary Applications 9(10):1205-1218.

Kim JY, Jeong S, Kim KH, Lim WJ, Lee HY, Kim N (2019). Discovery of Genomic Characteristics and Selection Signatures in Korean Indigenous Goats Through Comparison of 10 Goat Breeds. Frontiers in Genetics 10:438454.

Kirin M, McQuillan R, Franklin,CS, Campbell H, Mckeigue PM, Wilson JF (2010). Genomic runs of homozygosity record population history and consanguinity. PLoS One 5:e13996.

Liu D, Chen Z, Zhao W, Guo L, Sun H, Zhu K, Liu G, Shen X, Zhao X, Wang Q, Ma P, Pan Y (2021). Genome-wide selection signatures detection in Shanghai Holstein cattle population identified genes related to adaption, health and reproduction traits. BMC Genomics 22:1-19.

Liu Y, Zhao G, Lin X, Zhang J, Hou G, Zhang L, Liu D, Li Y, Li J, Xu L (2022). Genomic inbreeding and runs of homozygosity analysis of indigenous cattle populations in southern China. PLoS One 17(8):e0271718.

Marras G, Gaspa G, Sorbolini S, Dimauro C, Ajmone-Marsan P, Valentini A, Williams JL, Macciotta NP (2015). Analysis of runs of homozygosity and their relationship with inbreeding in five cattle breeds farmed in Italy. Animal Genetics 46(2):110-121.

Martinez AM, Gama LT, Canon J, Ginja C, Delgado JV, Dunner S, Landi V, Martin-Burriel I, Penedo MCT, Rodellar C, Vega-Pla JL, Acosta A, Alvarez LA, Camacho E, Cortés O, Marques JR, Martínez R, Martínez RD, Melucci L, Martínez-Velázquez G, Muñoz JE, Postiglioni A, Quiroz J, Sponenberg P, Uffo O, Villalobos A, Zambrano D, Zaragoza P (2012). Genetic footprints of Iberian cattle in America 500 years after the arrival of Columbus. PLoS One 7:e49066.

Medugorac I, Veit-Kensch CE, Ramljak J, Brka M, Marković B, Stojanović S, Bytyqi H, Kochoski L, Kume K, Grünenfelder HP, Bennewitz J, Förster M (2011). Conservation priorities of genetic diversity in domesticated metapopulations: a study in taurine cattle breeds. Ecology and Evolution 1(3):408-420.

Mulim HA, Brito LF, Pinto LF, Ferraz JB, Grigoletto L, Silva MR,

Pedrosa VB (2022). Characterization of runs of homozygosity, heterozygosity-enriched regions, and population structure in cattle populations selected for different breeding goals. BMC Genomics 23(1):209.

Murray C, Huerta-Sanchez E, Casey F, Bradley DG (2010). Cattle demographic history modelled from autosomal sequence variation. Philosophical Transactions of the Royal Society B: Biological Sciences 365(1552):2531-2539.

Peripolli E, Munari DP, Silva MVGB, Lima ALF, Irgang R, Baldi F (2017). Runs of homozygosity: current knowledge and applications in livestock. Animal Genetics 48(3):255-271.

Peripolli E, Metzger J, Antunes de Lemos MV, Stafuzza NB, Kluska S, Olivieri BF, Braga Feitosa FL, Piatto Berton M, Lopes FB, Munari DP, Lôbo RB, Magnabosco CU, Di Croce F, Osterstock J, Denise S, Cravo Pereira AS, Baldi F (2018a). Autozygosity islands and ROH patterns in Nellore lineages: evidence of selection for functionally important traits. BMC Genomics 19:1-14.

Peripolli E, Stafuzza NB, Munari DP, Lima ALF, Irgang R, Machado MA, do Carmo Panetto JC, Ventura RV, Baldi F, da Silva MVGB (2018b). Assessment of runs of homozygosity islands and estimates of genomic inbreeding in Gyr (Bos indicus) dairy cattle. BMC Genomics 19:1-13.

Pilon B, Hinterneder K, Hay EA, Fragomeni B (2021). Inbreeding calculated with runs of homozygosity suggests chromosome-specific inbreeding depression regions in Line 1 Hereford. Animals 11(11):3105.

Pryce JE, Hayes BJ, Goddard ME (2012). Novel strategies to minimize progeny inbreeding while maximizing genetic gain using genomic information. Journal of Dairy Science 95(1):377-388.

Purcell S, Neale B, Todd-Brown K, Thomas L, Ferreira MA, Bender D, Maller J, Sklar P, de Bakker PI, Daly MJ, Sham PC (2007). PLINK: a tool set for whole-genome association and population-based linkage analyses. American Journal of Human Genetics 81(3):559-575.

Purfield DC, Berry DP, McParland S, Bradley DG (2012). Runs of homozygosity and population history in cattle. BMC Genetics 13(1):1-11.

Saravanan KA, Panigrahi M, Kumar H, Parida S, Bhushan B, Gau GK, Dut T, Mishra BP, Singh RK (2021). Genomic scans for selection signatures revealed candidate genes for adaptation and production traits in a variety of cattle breeds. Genomics 113(3):955-963.

Scienski K, Ialacci A, Bagnato A, Reginelli D, Durán-Aguilar M, Strillacci MG (2019). Variabilidad genética en una población de vacas Holstein utilizando marcadores SNP y su uso para monitorear estrategias de apareamiento. Revista Mexicana de Ciencias Pecuarias 10(3):643-663.

Sumreddee P, Toghiani S, Hay EH, Roberts A, Aggrey SE, Rekaya R (2020). Runs of homozygosity and analysis of inbreeding depression. Journal of Animal Science 98(12):skaa361.

Szmatoła T, Gurgul A, Jasielczuk I, Ząbek T, Ropka-Molik K, Litwińczuk Z, Bugno-Poniewierska M. (2019). A comprehensive analysis of runs of homozygosity of eleven cattle breeds representing different production types. Animals 9(12):1024.

Toro-Ospina AM, Herrera Rios AC, Pimenta Schettini G, Vallejo Aristizabal VH, Bizarria dos Santos W, Zapata CA, Ortiz Morea EG (2022). Identification of Runs of Homozygosity Islands and Genomic Estimated Inbreeding Values in Caqueteño Creole Cattle (Colombia). Genes 13(7):1232.

Villalobos Cortés AI, Martínez AM, Escobar C, Vega-Pla JL, Delgado JV (2010). Study of genetic diversity of the Guaymi and Guabala bovine populations by means of microsatellites. Livestock Science 131(1):45-51.

Wright S (1922). Coefficients of inbreeding and relationship." The American Naturalist 56(645):330-338.

Wu PI, Ross C, Siegele DA, Hu JC (2021). Insights from the reanalysis of high-throughput chemical genomics data for Escherichia coli K-12. G3 11(1):jkaa035.

Zinovieva NA, Dotsev AV, Sermyagin AA, Deniskova TE, Abdelmanova AS, Kharzinova VR, Sölkner J, Reyer H, Wimmers K, Brem G (2020). Selection signatures in two oldest Russian native cattle breeds revealed using high-density single nucleotide polymorphism analysis. PLoS One 15(11):e0242200.

Related Journals: